Hydrogenation behavior in rectangular metal hydride tanks under effective heat management processes for green building applications

Gkanas, E, Khzouz, M, Panagakos, G, Statheros, T, Mihalakakou, P, Siasos, GI, Skodras, G & Makridis, SS

Original citation & hyperlink:
Gkanas, E, Khzouz, M, Panagakos, G, Statheros, T, Mihalakakou, P, Siasos, GI, Skodras, G & Makridis, SS 2017, 'Hydrogenation behavior in rectangular metal hydride tanks under effective heat management processes for green building applications' *Energy*, vol 142, pp. 518-530
https://dx.doi.org/10.1016/j.energy.2017.10.040

DOI 10.1016/j.energy.2017.10.040
ISSN 0360-5442
ESSN 1873-6785

Publisher: Elsevier

Accepted Manuscript

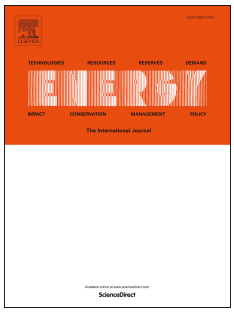

Hydrogenation behaviour in rectangular metal hydride tanks under effective heat management processes for green building applications

Evangelos I. Gkanas, Martin Khzouz, Grigorios Panagakos, Thomas Statheros, Panagiota Mihalakakou, Gerasimos Siasios, Georgios Skodras, Sofoklis S. Makridis

PII: S0360-5442(17)31709-7

DOI: 10.1016/j.energy.2017.10.040

Reference: EGY 11684

To appear in: *Energy*

Received Date: 27 March 2017

Revised Date: 5 October 2017

Accepted Date: 9 October 2017

Please cite this article as: Gkanas EI, Khzouz M, Panagakos G, Statheros T, Mihalakakou P, Siasios G, Skodras G, Makridis SS, Hydrogenation behaviour in rectangular metal hydride tanks under effective heat management processes for green building applications, *Energy* (2017), doi: 10.1016/j.energy.2017.10.040.

Hydrogenation behaviour in rectangular metal hydride tanks under effective heat management processes for green building applications

Evangelos I. Gkanas[1*], Martin Khzouz[1], Grigorios Panagakos[2], Thomas Statheros[1], Panagiota Mihalakakou[3], Gerasimos Siasios[1,3,4], Georgios Skodras[4], Sofoklis S. Makridis[3]

1. *Hydrogen for Mobility Lab, Centre for Mobility and Transport, Coventry University, Coventry University, Priory Street, Coventry, CV1 5FB, United Kingdom.*
2. *Environmental Research Laboratory, NCSR 'Demokritos', 15310 Athens, Greece*
3. *Department of Environmental and Natural Resources Management, University of Patras, 2 Seferi St. Agrinio, Greece*
4. *Novel & Clean Technologies Lab., Dept. of Mechanical Engineering, University of Western Macedonia, Mpakola & Sialvera, 501 00 Kozani, Greece*

[*]*Corresponding author email: evangelos.gkanas@coventry.ac.uk/egkanas@gmail.com*

Abstract

A fully validated with solid experimental results numerical study regarding the hydrogenation process of rectangular metal hydride beds under effective internal heat management is presented and analysed. Three different geometries equipped with plain embedded heat management tubes are introduced and examined. For each geometry, five different values of metal hydride thickness are studied and additionally, the effect of the coolant flow is examined in terms of different values of heat transfer coefficient [W/m^{2}K]. To evaluate the effect of the heat management process, a variable named as Non-Dimensional Conductance (NDC) is analysed and studied. Furthermore, three different materials are introduced, two "conventional" AB_5 intermetallics and a novel AB_2-based Laves phase intermetallic. According to the results, the optimum value for the metal hydride thickness was found to be 10.39 mm, while the optimum value for the heat transfer coefficient was 2000 [W/m^{2}K]. For the above optimum conditions, the performance of the novel AB_2-based Laves phase intermetallic showed the fastest hydrogenation kinetics compared to the other two AB_5 intermetallics indicating that is a powerful storage material for stationary applications.

Keywords: Hydrogen Storage; Heat Management; Stationary Applications; Heat and Mass Transfer; Green Buildings;

1. Introduction

There is an international need to promote innovative approaches for mitigation of carbon dioxide (CO_2) emissions due to energy consumption associated with building construction and operation [1, 2]. As the shift to low carbon electricity is rising, the electrification of buildings powered by low carbon processes should be amongst the main pillars of the approach efficiency – sufficiency – renewables [3]. With view to the sustainable performance of green buildings, the appropriate application of renewable energy supplies in buildings is fundamental criterion [4]. In this regard, solar sustainability systems have always been a key factor towards development of green buildings [5-7]. All modern cities must be greener and smarter; hence, promoting sustainable cities has become a key issue for all developing (and developed) countries [8]. Sustainability is a global concept comprising various interrelated studies about people, environment and society [9]. To emphasize the substantial negative impacts of buildings on the environment, we refer to a comprehensive analysis [10], presenting the respective impacts in US as shown in Figure 1; other rich and developed countries are believed to follow a similar trend.

Figure 1. Environmental impact of buildings [10]

One of the main outcomes of the aforementioned study is that the energy consumption and gas emissions are the most considerable negative consequences which require innovative solutions.

At the moment, in all developed countries, a significant amount of the total primary energy is consumed in buildings and can be reduced by adopting energy efficiency strategies using renewable sources [11, 12]. In fact, in the EU and US; energy consumption in buildings has even exceeded the energy consumption of the industrial and transportation sectors [13, 14]. Energy consumption in buildings accounts for around 20-40 % of all energy consumed in advanced countries. The future belongs to the Renewable Energy Sources (RES); defined as sources of energy that can be derived from natural processes, and to be constantly replenished [15]. There are four main electricity storage applications that can be distinguished for RES management: 1) Load Leveling, 2) Time Shifting, 3) Forecast optimization uses the storage system as a buffer enabling a real-time RES production and 4) Grid

stabilization and system services [16, 17]. Hydrogen technologies are assumed as powerful techniques for storage of RES since H_2 and O_2 can be stored and used to produce electricity in fuel cell systems where the O_2/H_2 fuel cells are air independent and present a more efficient output comparing to Air/H_2 fuel cells [18]. The coupling of such a fuel system with RES allows not only a partial building autonomy but also provides the function of backup system for several hours at high power; thus, the topic of efficient hydrogen storage and compression is of high interest and need further research [19]. Komiyama *et al*. [20] showed that the installation of hydrogen storage is promoted by both the cost reduction and the CO_2 regulation policy. In addition, hydrogen storage was found to be suitable for storing variable renewables (VR) energy in long periods of time.

The parameters that governs the performance of metal hydrides can be classified in two large categories: a) the material related parameters and b) operation/design related parameters [21, 22]. Some of the material related parameters are: the (specific) enthalpy of formation/deformation of the hydride ΔH [kJ/kmol], the specific heat capacity of the hydride C_p [kJ/kmol/K], the thermal conductivity λ [W/mK], hysteresis and slope [23]. Some of the operation/design related parameters are: the porosity of the metal hydride bed, the packing density, the operational temperatures, the geometry of the metal hydride vessel, the supply pressure and the heat management techniques.

There are also issues associated with the kinetic performance of hydrogen storage materials and mainly related to the storage capacity, the thermal stability of the hydride, the kinetics of hydrogenation and dehydrogenation, the thermo-physical properties and crystal structures of the candidate materials [24]. Specifically, fast reaction kinetics and high hydrogen storage capacity are probably the most important properties of the alloys used in thermal devices [25], compression systems [26-31] and heat pumps [32, 33].

The limiting factor that controls the hydrogen charging/discharging process in a metal hydride reactor is the rate of heat that is transferred to/from the reactor. Large amounts of heat are produced inside the reactor due to the exothermic nature of the hydrogenation process, forcing the equilibrium pressure to increase and thus the driving force for the hydrogen storage is reduced. On the other hand, large amounts of heat and consequently low internal pressure are crucial for an effective and fast dehydrogenation process. Thus, heat management of the metal hydride reactors is

necessary for effective hydrogen storage in metal hydrides. There are mainly two heat management techniques that have been applied to enhance the heat transfer to/from the metal hydride tank. These techniques are: internal heat management and external heat transfer [34-36].

According to Fourier's law of conduction, there are three ways to improve the heat transfer in the metal hydride bed; introduction of a large temperature difference [37, 38], reduction of the metal hydride thickness [39, 40] and/or thermal conductivity enhancement [41-45].

In the current study, a fully validated mathematical model with solid experimental results is introduced. The heat, mass and momentum transfer during the hydrogenation process of three different potential materials is examined. The materials used in the current study are: $LaNi_5$, $MmNi_{4.6}Al_{0.4}$ and a novel AB_2-*type* Laves phase intermetallic which presents easy and fast activation process and capability for usage in stationary applications. The metal hydride beds used in the current work are of rectangular shape and various internal heat management scenarios also considered. The heat management consist of several plain embedded heat management tubes distributed within the geometries. Three different geometries using different distribution of the tubes are analysed and examined. For each geometry introduced, five different values of metal hydride thickness are studied and additionally, the effect of the coolants flow is examined in terms of different values of heat transfer coefficient [W/m^2K]. To evaluate the effect of the heat management process, a variable named as Non-Dimensional Conductance (NDC) is analysed and studied. After the optimization process is being identified, the optimum geometries were taken into account and the performance of all the suggested materials is compared.

2. Methodology

In the current study, the rectangular reactor performances were modeled in a commercial multiphysics software (COMSOL Multiphysics 5.0) by solving simultaneously the heat, mass and momentum conservation equations. Prior to conducting these simulation runs the performance of the proposed numerical model was validated using solid experimental results extracted from a lab-scale Sievert's type apparatus for both the hydrogen storage capacity and the temperature distribution

within the hydride. The expansion of packed beds during the hydrogenation process can produce additional stress on the vessel walls; therefore, for the purpose of the model, the reactors are assumed to be filled to 50% at the beginning of the hydrogenation process. After the validation process, the simulation runs were conducted for all the suggested geometries, the different materials and values of the heat transfer coefficient and the most optimum cases were obtained.

2.1 Model Assumptions

A number of assumptions were made which serve to simplify the modeling process and listed as follows:

a) Initially uniform temperature and pressure profiles.

b) Hydrides thermal conductivity and specific heat capacity are assumed constant during the hydrogenation process. The specific heat capacity is very difficult to measure experimentally; particularly near to the phase change conditions and therefore a large error is introduced. The thermal conductivity of the hydride depends on the hydrogen concentration, the pressure and the temperature, varying as well as an order of magnitude. However, when an effective heat management if being applied (addition of high thermal conductivity materials such as aluminum foams, internal heat management *etc.*) the hydride thermal conductivity becomes irrelevant and the overall effective conductivity can be considered as constant [46]

c) The medium is in local thermal equilibrium which implies that there is no heat transfer between solid and gas phases

d) Hydrogen is treated as an ideal gas from a thermodynamic point of view.

e) The bed void fraction remains constant and uniform throughout the reaction.

f) The characteristics (the kinetics and thermal properties) of the bed are unaffected by the number of loading and unloading cycles. Thus, the bed aging is neglected.

g) The metal hydride bed fills the entire space between the cooling tubes (perfect packing condition).

2.2 Heat equation

Assuming thermal equilibrium between the hydride powder and hydrogen gas, a single heat equation is solved instead of separate equations for solid and gas phases:

$$(\rho \cdot Cp)_{eff} \cdot \frac{\partial T}{\partial t} + (\rho_g \cdot C_{p_g} \cdot \overline{v}_g) \cdot \nabla T + \nabla \cdot (\mathrm{k}_{\mathrm{eff}} \cdot \nabla T) = \mathrm{Q}_H \qquad (1)$$

The term Q_H *(W/m^3)* in Eq. 1 represents the heat that has been generated during the hydrogenation process or the amount of heat that is necessary for the dehydrogenation process. The amount of heat that is been produced during the hydrogenation process depends on several thermophysical properties of the materials such as the enthalpy of formation *ΔH (J/mol)*, the porosity of the material *ε*, the density change during the reaction (kg/m^3), the reaction rate (1/s) and the molecular mass of the stored gas (kg/mol) [47, 48]. The enthalpy of the hydride formation was measured experimentally from the isotherm curves for all the presented samples, while the density change was calculated and updated with time from the concentration of the species using the Transport of Diluted Species Module in COMSOL Multiphysics.

The effective heat capacity is given by;

$$(\rho \cdot Cp)_{\mathrm{e}} = \varepsilon \cdot \rho_g \cdot C_{pg} + (1-\varepsilon) \cdot \rho_s \cdot C_{ps} \qquad (2)$$

and the effective thermal conductivity is given by;

$$k_e = \varepsilon \cdot k_g + (1-\varepsilon) \cdot k_s \qquad (3)$$

The terms ρ_g, C_{pg}, C_{ps} and m refer to the density of the gas phase (kg/m^3), the specific heat capacity of the gas phase (J/kg/K), the heat capacity of the solid phase and the kinetic term for the reaction respectively. The parameter that represents the void fraction is symbolized with ε. M_{H2} represents the molecular mass of hydrogen (kg/mol) and T represents the temperature (K).

2.3 Hydrogen Mass Balance

The equation that describes the diffusion of hydrogen mass inside the metal matrix is given by:

$$\varepsilon \cdot \frac{\partial(\rho_g)}{\partial t} + div(\rho_g \cdot \vec{v}_g) = \pm Q \qquad (4)$$

Where, (-) refers to the hydrogenation process and (+) to the dehydrogenation process, v_g is the velocity of gas during diffusion within the metal lattice (descripted in

chapter 2.4) and Q is the mass source term describing the amount of hydrogen mass diffused per unit time and unit volume in the metal lattice.

2.4 Momentum equation

The velocity of a gas passing through a porous medium can be expressed by Darcy's law. By neglecting the gravitational effect, the equation which describes the velocity of gas inside the metal matrix is given by:

$$\vec{v}_g = -\frac{K}{\mu_g} \cdot grad(\vec{P}_g) \tag{5}$$

Where K is the permeability of the solid and μ_g is the dynamic viscosity of gas and P_g is the pressure of gas within the metal matrix.

2.5 Kinetic expression

The kinetic description for the hydrogenation process per unit time and volume is described by the following equation:

$$m_a = C_a \cdot \exp[-\frac{E_a}{R_g \cdot T}] \cdot \ln[\frac{p_g}{P_{eq}}] \cdot (\rho_{ss} - \rho_s) \tag{6}$$

The amount of hydrogen released from the hydride bed is given by;

$$m_d = C_d \cdot \exp[-\frac{E_d}{R_g \cdot T}] \cdot (\frac{P_{eq} - p_g}{P_{eq}}) \cdot \rho_s \tag{7}$$

Where ρ_s and ρ_{ss} are the density of the hydride at any time and at saturation state respectively. C_a *(1/s)* and C_d *(1/s)* refer to the pre-exponential constants for the hydrogenation and dehydrogenation process and the E_a *(J/mol)* and E_d *(J/mol)* are the activation energy for hydrogenation and dehydrogenation process respectively.

The constants C_a and C_d as well as the activation energies for both the hydrogenation process and the dehydrogenation E_a and E_d are calculating from the experimental results. The first step is to obtain the kinetics of the hydrogenation and dehydrogenation process at several temperatures, and the next step is the design of the Vant Hoff plot (lnP vs 1/T). From the slope of the plot the activation energy can be extracted and from the intersect of the plot with the y-axis the constant can be also calculated [49, 50]. The saturation density is determined by calculating the hydride concentration (mol/m^3) after the storage process and the volume of the hydride after

the expansion process that occurs during the hydrogenation. As for the density of the hydride anytime, from the '*Transport of diluted species*' Module in COMSOL Multiphysics, the concentration of the hydride anytime is calculated (mol/m^3) and subsequently is substituted in Eq. (6) in order to calculate the kinetic term for the hydrogenation process

2.6 Equilibrium Pressure.

To incorporate and consider the effect of hysteresis and the plateau slope for the calculation of the plateau pressure P_{eq}, the following equation was used [51, 52]:

$$\ln\frac{P_{eq}}{10^5}=\left\{\left[\frac{\Delta H}{RT}-\frac{\Delta S}{R}\right]+\left(\varphi_s\pm\varphi_0\right)\cdot\tan\left[\pi\cdot\left(\frac{x}{x_{sat}}-\frac{1}{2}\right)\right]\pm\frac{S}{2}\right\} \quad (8)$$

The plateau slope is given by the flatness factors φ_s and φ_0 and S represents the hysteresis effect which is given by ($\ln P_{abs}/P_{des}$) designated '+' for hydrogenation and '-' dehydrogenation, while x and x_{sat} are the local hydride concentration at any given time and at saturation respectively. For all the studied materials, the flatness factors and the hysteresis effects were measured experimentally by using the data collected from the hydrogenation kinetics and isotherms.

3. Validation of numerical results

To investigate the validity the proposed numerical model, experiments were performed on a 0.7g sample of $LaNi_5$ powder synthesized by arc melting. After the bulk buttons were synthesized for the first time, they turned and the melting process was repeated at least three more times in order to assure the homogeneity of the synthesized samples. The phase purity was validated using means of XRD (Rietveld Analysis). The pressure-composition-isotherm (PCI) hydrogenation measurements were performed on a commercial Sievert type apparatus provided by HIDEN Isochema (IMI Instruments). Both the hydrogenation behavior and the temperature behavior of the material were recorded during the charging process at an initial hydrogen supply pressure of 15 bar. Figure 2a shows the reactor geometry used for the current validation process and the position of the thermocouple as well. Furthermore, in order to validate the hydrogenation and temperature behavior of the AB_2-type Laves phase alloy, experiments were performed on a large-scale metal

hydride tank, equipped with 850g of powder on a cylindrical tank. The tank geometry used in the current case and the thermocouple are presented in Figure 2b.

Figure 2. Geometries used for the validation of the numerical model. Figure 2a shows the geometry used for the validation of $LaNi_5$ and the position of the thermocouple and Figure 2b shows the geometry used for the validation of the AB_2-intermetallic.

The experiments for the validation process of the AB_2 intermetallic were performed on a lab scale Sievert-type apparatus with a capacitance manometer (Druck PTX 620) at starting temperature 20^{o}C and supply pressure 30 bar. Figure 3a shows the comparison of the temperature profile during the hydrogenation process and Figure 3b shows the hydrogenation profile for $LaNi_5$. The validation of the temperature and the hydrogenation profile of the AB_2-intermetallic are presented at Figure 3c and 3d respectively. The results of the numerical work compared to the experimental data present good agreement with a maximum deviation of less than 5%.

Figure 3. Validation of the predicted amount of hydrogen stored (3a) for different temperatures and different pressures and released (3b) for two different temperatures with experimental data extracted from a lab scale Sievert type apparatus. Fig 1c shows the validation of the temperature profile of the AB_2-intermetallic and Fig. 1d presents the validation of the hydrogenation behavior of the same material. The experimental results (dots) with the simulation results (lines) are in good agreement with a maximum deviation less than 5%.

Furthermore, to ensure that the proposed numerical model is capable to describe the effect of the convective heat transfer during the hydrogenation process, an additional validation process was performed with the results published by Muthukumar *et al*. [53]; they studied the effect of the convective heat transfer during the installation of several co-central cooling tubes on a metal hydride bed. The material used in that study had the characteristics of $MmNi_{4.6}Al_{0.4.}$ Figure 4a shows the comparison between the results of the present work and the results extracted by [53] for the average temperature evolution within the metal hydride bed during the hydrogenation process for the case of using 12-16 and 20 cooling tubes (the geometries are embodied). Furthermore, Figure 4b shows the bed average hydrogenation capacity during the charging process for the same number of cooling tubes (12-16 and 20). The results are in good coherence between the two studies, indicating that the suggested numerical model is valid while describing the convective heat transfer.

Figure 4. Validation of the proposed numerical model regarding the ability to predict the convective heat transfer with the results published by Muthukumar et al. [53]. Figure 4a presents the comparison of the average bed temperature and Figure 4b presents the comparison of the average hydrogenation capacity.

4. Tank Design Geometries

The metal hydride tanks were selected to be of rectangular shape; the properties of stainless steel (316 SS) with wall thickness of 3mm selected. The dimensions of each tank were 30•15•12.63 cm corresponding to a net volume of 5683.5 cm^3. The tubes are placed along the 15-cm side of the rectangular and their length is 30cm. The reason for this settlement is to ensure that the cooling path for the coolant is enough to cause effective cooling of the tank during the hydrogenation process.

Figure 5 presents the cross sections of the three different geometries used. Figure 5a presents the first geometry (Geometry 1) where a single row of tubes is placed within the tank. Figure 5b and 5c present the next two geometries used (Geometry 2 and Geometry 3) where a double row and a mixed-row of tubes are taken into account. The heat management tubes selected for the current study selected to present the same properties and dimensions with commercial available ¼ inch stainless steel tubes.

Figure 5. Cross-section of the three heat management geometries. Figure 5a shows the first geometry with a single row of tubes (Geometry 1). Figure 5b presents the second geometry with double row of cooling tubes (Geometry 2) and Figure 5c shows the third geometry (Geometry 3) with a mixed tube arrangement.

4.1 Optimization Factors and Control Parameters

The charging/discharging time is of major importance for the effective performance of a metal hydride tank. The purpose of the present optimization process is to obtain the parameters of the systems that lead to the minimum charging/discharging time (t_s). In the current work, the charging/discharging time (t_s) is defined as the time required for the average reacted fraction to rise from 0.1 to 0.9 during the hydrogenation process. The parameters examined in the current work are: a) the metal hydride thickness *L(mm)* and b) the coolants flow within the tubes which is represented by the heat transfer coefficient h_t *(W/m^{2}K).*

Table 1 presents all the control factors and the values used for the current study.

Table 1. Control factors used for the optimization process

4.2 Non-Dimensional Conductance (NDC)

The reaction rate for the hydrogenation/dehydrogenation depends on the heat transfer parameters. In the current work, heat exchangers are used to enhance the hydrogenation behavior of several metal hydrides under several heat management conditions. When using a heat exchanger, there are several parameters that influence the rate of heat transfer such as the coolant temperature, coolant flow rate, contact resistance, metal hydride thickness and the thermal conductivity of the metal hydride bed. To monitor the influences of the above parameters on the heat transfer performance a Non-Dimensional Conductance (NDC) parameter can be used [40]. The NDC is defined as the ratio of the maximum heating rate that can be removed from the metal hydride to the heat rate that would be generated for a specified thickness of the hydride to store hydrogen up to 90% of its maximum theoretical performance during a desirable time and its given by the following expression.

$$NDC = \frac{\left(\frac{T_{MH,\max} - T_{cool}}{\frac{1}{h_t} + R_{tc} + \frac{L}{\lambda}} \right)}{\left(\frac{\Delta H \cdot (\mathrm{wt}\,\%) \cdot \rho}{MW_{H2}} \cdot \frac{L}{t_{des}} \right)} \tag{9}$$

Higher values of NDC result in larger heat transfer rates. $T_{MH,max}$ *(K)* is the temperature of the metal hydride at the end of the pressure increase process and it's an indirect measurement of the pressure. T_{cool} *(K)* is the temperature of the coolant that flows within the heat management tubes and a higher NDC number can be achieved by reducing the coolant temperature. The heat transfer coefficient is represented by h_t *(W/m^{2}K)* and is directly related to the effect of the coolant flow rate. R_{tc} *(mm^{2}K/W)* is the contact resistance between the metal hydride powder and the wall of the heat management tubes and it depends on the hydride powder properties (grain size and packing density). *L (mm)* is the hydride layer thickness as shown in Figure 6a. In the current work, the metal hydride thickness is defined as the distance between the

centers of two adjacent coolant tubes and consists of the metal hydride, the contact resistance and the wall of the coolant tube as shown in Figure 6b. The denominator in Eq. 9 is the average heat generation rate if the metal hydride of thickness L is hydride within a desired filling time t_{des}. In the current analysis, the desired time t_{des} is selected 2000s.

Figure. 6 Definition of the metal hydride thickness. Figure 6a shows the metal hydride thickness defined as the distance between the centers of two adjacent tubes. Figure 6b shows that the metal hydride thickness consists of the tube wall, the contact resistance and the metal hydride.

5. Results and Discussion

5.1 Hydrogenation behavior of $LaNi_5$

The initial temperature of the materials for all cases prior the hydrogenation process was 20^{o}C and the initial temperature of the coolant was also 20^{o}C. Hydrogen supply pressure was 15 bar; the pressure that a commercial electrolyser can supply. Three different geometries were studied named as ***Geometry 1***, ***Geometry 2*** and ***Geometry 3*** based on the way that the cooling tubes are placed inside the tank. Furthermore, for each geometry, five values of hydride bed thickness were examined: *14.39/12.11/10.39/9.01/7.89* mm. For each value of thickness, five different coolant flow rates represented by the overall heat transfer coefficient were considered. Out of the mathematical point of view, the heat transfer coefficient is the ratio between the heat flux to the temperature change. This temperature change ΔT is the driving force for the transfer of the thermal energy. The coefficient of performance depends on various factors such as the geometry, the flow regime, the fluid to wall temperature ratio and the fluids thermophysical properties such as heat capacity, density, viscosity and thermal conductivity. Figure 7 presents the hydrogenation response of $LaNi_5$ in respect to different values for the heat transfer coefficient h_t *= 200, 500, 1000, 2000 and 5000 [W/m^{2}K]* for *Geometry 1* [single row of cooling tubes]. For all the different cases of the metal hydride thickness *(14.39/12.11/10.39/9.01/7.89* mm*)*, the evolution of the time that the hydride needs to reach the hydrogenation fraction X=0.9 for all the different values of the heat transfer coefficient present an almost parabolic behavior until the value of h_t=2000 [W/m^{2}K] while for higher values (5000 [W/m^{2}K]) the behavior becomes almost linear, showing non-significant change in the charging time. This behavior indicates a limitation mechanism in the reduction of the hydrogenation

time with the increase of the heat transfer coefficient over a certain value. For lower values, a slightly change seems to affect hardly the hydrogenation behavior, but for higher values of the coefficient this phenomenon is limited.

Figure 7. Hydrogenation response of $LaNi_5$ when using Geometry 1 for the heat management process, for all the different metal hydride thicknesses and all the values of the heat transfer coefficient.

The same results as explained above are observed both for the case of using Geometry 2 and Geometry 3 in terms that they present the same trend on the effect of the heat transfer coefficient and the metal hydride thickness. The overall heat transfer coefficient in the case of the heat management of metal hydride tanks, takes into account the convective heat transfer resistance between the coolant and the tube wall, the conductive resistance between the inner reactor wall and the hydride powder (the hydride particles). Thus, the behavior of the performance of the hydrogenation process with the values of the heat transfer coefficient can be explained with the fact that due to the internal heat transfer constraint imposed by the low thermal conductivity of the hydride bed and the relatively high thermal resistance of the wall, the increase of the heat transfer coefficient over a certain value, does not have a significant effect on the hydrogenation time.

Figure 8 presents the variation of the hydrogenation time with the Non-Dimensional Conductance (NDC) for all the values of the heat transfer coefficient and the hydride thickness. Figure 8a shows the variation for Geometry 1 (single row tubes), while Figure 8b and 8c presents the variation for Geometry 2 (double row tubes) and Geometry 3 (mixed tubes) respectively. The hydride thickness reduces from 14.39 to 7.89 mm and the convective heat transfer coefficient varies from 200-5000 W/m^2K as presented in Table 1. For all the geometries, the time to reach X=0.9 decreases almost monotonically with an increase of the heat transfer coefficient. For certain values of metal hydride thickness, increasing the convective coefficient from 200 to 500 W/m^2K can significantly reduce the hydrogenation time to reach X=0.9 over 1200s. Furthermore, when increasing the convective coefficient higher than 2000 W/m^2K does not lead to any significant improvement (less than 5%) of the hydrogenation time, confirming the findings that described earlier. From Figure 8 the slope of the same hydride thickness groups decreases in correlation to the hydride thickness. Therefore, this implies that the difference in the hydrogenation time while in region of

the heat transfer coefficient of 200 W/m^{2}K – 500 W/m^{2}K is more significant in lower values of metal hydride thicknesses.

Figure 8. Variation of the charging time with the NDC. Figure 8a shows represents the behavior of Geometry 1, while Figure 8b and 8c shows the behavior of Geometry 2 and 3 respectively.

5.2 Hydrogenation Behavior of $MmNi_{4.6}Al_{0.4}$ and the AB_2 based intermetallic

The second material studied in the current work is $MmNi_{4.6}Al_{0.4}$. The reason for choosing such material is the need to improve the degradation behavior of the hydrogenation capacity over long term cycling. $LaNi_5$ can experience a reduction in capacity over 50 % after almost 550 charging/discharging cycles at a temperature near 500 K [34], so the addition of a small fraction of Al instead of Ni seems a promising solution. Figure 9a shows the hydrogenation response when $MmNi_{4.6}Al_{0.4}$ is considered as the operating hydride in respect to different values of the heat transfer coefficient h_t*=200, 500, 1000, 2000 and 5000 [W/m^{2}K]* for the case of Geometry 2 [double row of cooling tubes].

Figure 9. Hydrogenation response of $MmNi_{4.6}Al_{0.4}$ (9a) and the AB_2-intermetallic (9b) when using Geometry 2 for the heat management process, for all the different metal hydride thicknesses and all the values of the heat transfer coefficient.

According to the results for all the different values of metal hydride thickness, the evolution of the hydrogenation time for different heat transfer coefficients until the value of h_t*=2000* [W/m^{2}K] present a parabolic behavior in agreement with the behavior described for the performance of $LaNi_5$. As also expected, after the value of h_t*=2000* [W/m^{2}K] the behavior becomes linear and no significant change in the hydrogenation response is obtained as also the thermal conductivity of $MmNi_{4.6}Al_{0.4}$ is low and prevent the effective heat transfer between the hydride particles and the tube walls in addition with the thermal resistance of the walls are introducing this limitation on the drop of the hydrogenation time after a certain value of the overall heat transfer coefficient.

The third material studied in the current work is a novel AB_2 Laves phase intermetallic that has been synthesized by levitation melting and its thermophysical

properties have been tested experimentally. The intermetallic exhibits improved hydrogen storage properties at ambient temperature and relatively moderate pressure range (10-15 bar). The hydrogen storage properties of this material have been obtained experimentally using a lab-scale Sievert-type apparatus. Figure 9b shows the hydrogenation response when the AB_2 intermetallic is considered as the operating hydride in respect to different values of the heat transfer coefficient h_t*=200, 500, 1000, 2000 and 5000 [W/m*^{2}*K]* for the case of Geometry 2 [double row of cooling tubes].

The hydrogenation behavior of this material for all the cases of metal hydride thickness presents the same parabolic trend for the lower heat transfer coefficient values and after a certain point the behavior becomes linear. From the previous analysis and observations, the optimum value of the heat transfer coefficient is selected at h_t=2000 [W/m^{2}K] for the further optimization of the system.

5.3 Effect of the metal hydride thickness on the hydrogenation behavior of the studied materials

According to the analysis described in the previous chapter, the optimum value for the overall heat transfer coefficient was selected to be 2000 [W/m^{2}K]. By keeping this value constant, a comparison study is performed for all the selected materials in terms on the effect that metal hydride thickness adds on the hydrogenation behavior. Figure 10a presents the hydrogenation behavior of $LaNi_5$ for all the geometries (Geometry 1, 2 and 3) and the metal hydride thicknesses *(14.39/12.11/10.39/9.01/7.89* mm*)*.

Figure 10. Effect of the metal hydride thickness on the hydrogenation behavior of $LaNi_5$. Figure 10a shows the comparison of the hydrogenation behavior of all the geometries for all the possible metal hydride thicknesses and Figure 10b shows the hydrogenation process with the NDC.

As the metal hydride thickness drops (thus, the number of the cooling tubes within the hydride increases) the hydrogenation process becomes faster. For the case of using Geometry 1 (single row cooling tubes) as the thickness decreases from 14.39 mm to 12.11 mm the time for the material to reach the hydrogenation fraction X=0.9 reduces by almost 4.5min (265s). By further reduction of the thickness to 10.39 mm the hydrogenation response drops another 2.5 min (163s). A further decrease to 9.01 mm reduces the hydrogenation time to 1.5 min (99s) and the reduction to a thickness of

7.89 mm results to a very small drop of less than a minute (54s). When using the Geometry 2 [double row of cooling tubes], the hydrogenation behavior follows almost the same trend as the one presented for Geometry 1, but in that case, it seems that after the metal hydride thickness of 10.39 mm, there is no significant decrease on the hydrogenation response of $LaNi_5$ for any further reduction of the thickness. This behavior of Geometry 2 indicates a limitation on the maximum number of cooling tubes or in other words a limitation on the effect of the heating/cooling path within the metal hydride. Finally, for the Geometry 3 (mixed row of cooling tubes) the behavior is slightly different as seen in Figure 10a. The reason for this kind of behavior lies on the nature of the Geometry 3. As explained in Table 1, the thickness of 14.31 mm corresponds to 12 cooling tubes and the thickness of 12.11 mm corresponds to 13 tubes, while for further reduction to thickness 10.39 mm the number of tubes increases by two and the total number of tubes is 15. The number of cooling tubes for the thickness of 9.01mm is 16 and for the 7.89 mm is 18, resulting to the faster drop for the case of thickness 10.39 and 7.89 mm comparing to the rest of the cases due to the fact that the total amount of heat exchangers is larger.

Figure 10b presents the variation of the hydrogenation with the Non-Dimensional Conductance (NDC) for the case of $LaNi_5$ as the operating material; for all the different geometries and the values for the metal hydride thickness. For Geometry 1 the results showed that as the hydride thickness drops, the hydrogenation behavior is faster and at the same time the NDC rises indicating an effective cooling process while increasing the number of the cooling tubes. This can be explained from the physical meaning of the NDC as defined in Eq. 9. While decreasing the hydride thickness, it is expected that the maximum temperature during the hydrogenation will be lower, resulting in a larger pressure ramp and a larger driving force for the storage. Furthermore, as the metal hydride thickness becomes lower, the numerator in Eq. 9 will increase resulting on the more effective removal of the generated thermal energy. The same trend is extracted for the behavior of Geometry 2 and 3. Though, for all the cases there is a limitation on the hydrogenation and heat management performance when the metal hydride thickness drops below 10 mm, where no significant difference is observed. This trend is possible related to the fact that the cooling path within the hydride becomes small and the effect of the convective heat transfer is eliminated. Furthermore, the poor conductivity properties of the hydrides are contributing in this limitation.

Figure 11 presents the performance of $MmNi_{4.6}Al_{0.4}$ during the hydrogenation process for Geometries 1, 2 and 3 with the different values of metal hydride thickness (Figure 11a) and with the NDC (Figure 11b). For Geometries 2 and 3 the results also showed that below the metal hydride thickness of 10.39 mm there is no significant effect on the filling time, while for Geometry 1 this limitation is eliminated and almost a straight behavior is observed.

Figure 11. Effect of the metal hydride thickness on the hydrogenation behavior of $MmNi_{4.6}Al_{0.4}$. Figure 11a shows the comparison of the hydrogenation behavior of all the geometries for all the possible metal hydride thicknesses and Figure 11b shows the hydrogenation process with the NDC.

Figure 12a and 12b present the behavior of the AB_2 Laves phase intermetallic during the hydrogenation process for all the different geometries. For all the geometries, any further reduction of the metal hydride thickness from 10.39 mm does not affect significantly the operation of the hydride.

Figure 12. Effect of the metal hydride thickness on the hydrogenation behavior of the AB_2 Intermetallic. Figure 12a shows the comparison of the hydrogenation behavior of all the geometries for all the possible metal hydride thicknesses and Figure 12b shows the hydrogenation process with the NDC.

5.4 Hydrogenation behavior of the different materials under the optimum operational conditions

Figure 13 presents the hydrogenation behavior of the different materials used in the current study for the three geometries considered when the storage process was studied under the optimum conditions obtained in the previous chapters (h_t=*2000 W/m^{2}K* and *L=10.39 mm*).

Figure 13. Comparison of the hydrogenation behavior of the three materials and all geometries when using the optimum values of h_t=2000[W/m^{2}K] and L=10.39mm

When using $LaNi_5$ as the operating material the time needed for the hydrogenation process to reach X=0.9 for using Geometry 1 is almost 3600 s (60 min), while for the case of Geometry 2 the corresponding time decreases to 2100 s (35 min) and for the case of Geometry 3 the required time is almost 2600s (44 min). When using

$MmNi_{4.6}Al_{0.4}$ for Geometry 1 the hydrogenation time is around 5700 s (90 min), while for the case of Geometry 2 the required time reduces to 3500s (58 min) and for the Geometry 3 the time is 4650 s (75 min).

Finally, when using the AB_2 alloy as the operating hydride, for the case of Geometry 1 the time for the hydrogenation process to reach X=0.9 is 2800 s (47 min), for the case of Geometry 2 the time reduces to 1560 s (26 min) and finally for the Geometry 3 the time is 2000 s (34 min).

For Geometry 1, the AB_2 alloy presents the fastest response comparing to both $LaNi_5$ and $MmNi_{4.6}Al_{0.4}$ by almost 14 and 48 min respectively. For Geometry 2 the AB_2 alloy is faster by almost 10 and 30 min to $LaNi_5$ and $MmNi_{4.6}Al_{0.4}$ respectively and finally for Geometry 3 the AB_2 alloy is faster by 11 and 45 min to $LaNi_5$ and $MmNi_{4.6}Al_{0.4.}$ It is clear from the results that the AB_2 Laves phase alloy presents the fastest reaction time during the hydrogenation process comparing to the two 'conventional' AB_5 alloys. This kind of behavior is explained by the thermophysical properties of the AB_2 alloy, such as the thermal conductivity, where according to the measurements performed it presented the highest of all the synthesized powders (λ_{AB2} = 1.15 W/mK) and the specific heat capacity which allows the heat transfer to be more efficient between the system coolant – tube walls – hydride powder.

Figure 14a presents the comparison of the reaction progress at the end of the desired time (2000s) for the Geometry 1 for the three studied materials and for all the different values of the metal hydride thickness when the heat transfer coefficient is h_t=2000 [W/m^{2}K]. The results showed that a charging time of 2000s is not achievable for all the materials when using Geometry 1 since all reaction progress values fall below 90% (X=0.9). Figure 14b showed the filling progress at the end of the desired time for the Geometry 2. In that case, $LaNi_5$ is able to achieve X=0.9 for the cases of thickness 9.01 and 7.89 mm, while for the AB_2 intermetallic the target of filling within 2000s is achieved for all the different cases of metal hydride thickness. For $MmNi_{4.6}Al_{0.4}$ is impossible to reach a filling time of X=0.9 within 2000s. Finally, Figure 14c shows the filling progress within 2000s for the case of Geometry 3. $LaNi_5$ is impossible to reach a filling of 90% within 2000s and the same results are extracted for the case of $MmNi_{4.6}Al_{0.4.}$ For the case of the AB_2 intermetallic is possible to achieve the target for the filling time only when the metal hydride thickness values are below 10.39 mm.

Figure 14. Comparison of the reaction fraction at the end of the desired charging time with the NDC. Figure 14a presents the comparison for Geometry 1, while Figure 14b and c for the Geometry 2 and 3 respectively.

5.5 Kinetics of the hydrogenation process

Figure 15a presents the bed average temperature evolution of the hydrides during the hydrogenation process for the case of Geometry 2 under the optimum operational conditions. The temperature at the beginning of the hydrogenation process increases due to the highly exothermic process and reaches a maximum point. After that, due to the heat management process the temperature drops and tends to reach the temperature of the coolant. For the cases of using $LaNi_5$ and the AB_2 alloy, the temperature evolution follows almost the same pattern, but the temperature of AB_2 decreases faster than the case of $LaNi_5$. The temperature evolution of $MmNi_{4.6}Al_{0.4}$ follows a slightly different pattern due to the different thermal properties that exhibits, though the temperature drop is slower to both the cases of $LaNi_5$ and $MmNi_{4.6}Al_{0.4.}$ The temperature behavior affects the hydrogenation kinetics as they presented in Figure 15b. Since the cooling process in the AB_2 alloy is more efficient it will reflect on the hydrogenation kinetics comparing to kinetics of $LaNi_5$ and $MmNi_{4.6}Al_{0.4.}$ The hydrogenation process can be categorized in two stages. During the first stage, the hydrogenation rate increases rapidly due to the large pressure difference between the pressure of the gas and the equilibrium pressure which acts as the driving potential for the hydrogenation process. The temperature for $LaNi_5$ and AB_2 rises rapidly and reaches a maximum of 66-68 ^{o}C during the first 150s of the reaction due to the low thermal conductivity of the hydride powders that restrict to the effective heat removal, and at that time the hydride stores an amount of hydrogen at a hydrogenation fraction X=0.18 (18% of the theoretical maximum amount of hydrogen that can be stored). During the first stage of the hydrogenation process, the pressure difference is the major factor for the rapid storage. The temperature rise increases the equilibrium pressure and as a result, the driving potential for the hydrogenation process decreases; during the second stage of the hydrogenation the circulating coolant removes the produced heat from the tank and reduces the temperature. As a result, the driving potential starts to increase and further storage takes place and this process continues

until the maximum capacity achieved. Thus; during the second stage of the hydrogenation process the heat transfer plays the major role.

Figure 15. Average temperature evolution (15a) and average hydrogenation fraction evolution (15b) for all the materials when using Geometry 2 and metal hydride thickness of 10.39 mm at a heat transfer coefficient value of 2000 [W/m^{2}K].

6. Conclusions

The work presented in this paper discusses the heat management of rectangular metal hydride tanks. A mathematical model, including the heat, mass and momentum conservation equations was proposed. A validation process with experimental results took place. For the validation needs, the storage behavior, the temperature distribution and the heat transfer during the hydrogenation were considered. Three heat management scenarios were investigated under variable values of metal hydride thickness (*14.39 – 12.11 – 10.39 – 9.01 and 7.89 mm*) and coolant flow rate (*200 – 500 – 1000 – 2000 – 5000 W/m^{2}K*). An optimum metal hydride thickness (10.39 mm) and coolant flow (2000 W/m^{2}K) were obtained. These results were found to be in good agreement with other studies that have been conducted on a similar topic [36, 40].

In addition, three different materials (*$LaNi_5$, $MmNi_{4.6}Al_{0.4}$ and AB_2-intermetallic*) for stationary hydrogen storage were examined. For each of the studied materials, the hydrogen storage kinetic behavior and temperature distribution during the hydrogenation were considered. Additionally, a Non-Dimensional Conductance parameter was introduced for the evaluation of the heat management. The results of the hydrogenation behavior of the introduced materials showed that the AB_2-intermetallic could store over 90% of the theoretical amount of hydrogen in less than 30 min. Therefore, in this study is highlighted that the performance of the AB_2 is superior to the $LaNi_5$ and $MmNi_{4.6}Al_{0.4}$, as far it concerns faster storage kinetics as a result of effective heat management.

Acknowledgements

The authors wish to thank Dr. Ahmad El-kharouf, School of Chemical Engineering, University of Birmingham for his valuable comments on the manuscript.

Nomenclature

C_a	*Absorption Reaction Constant, s^{-1}*
C_d	*Desorption Reaction Constant, s^{-1}*
C_p	*Specific Heat, J/kg-K*
E_a	*Activation Energy for Absorption, $J/molH_2$*
h	*Heat Transfer Coefficient, W/m^2K*
k	*Thermal Conductivity, W/m-K*
K	*Permeability, m^2*
M	*Molecular Weight, kg/mol*
m	*Kinetic Expression*
n	*Number of Hydrogen Moles*
P	*Pressure, bar*
R	*Gas Global Constant, J/mol-K*

Subscripts

a	*Absorption*
d	*Desorption*
e	*Effective*
eq	*Equilibrium*
f	*External Cooler*
g	*Gas*
i	*Initial*
s	*Solid*
ss	*Saturation*

Greek Letters

ε	*Porosity*
μ	*Dynamic Viscosity, kg/ms*

t	***Time (s)***	**ρ**	***Density, kg/m3***
T	***Temperature (K)***	**ΔH**	***Reaction Enthalpy, J/mol***
v	***Gas Velocity, m/s***	**ΔS**	***Reaction Entropy, J/mol-K***
V	***Volume, m^3***		

References

[1] Ghaffarian Hoseini A, Dahlan ND, Berardi U, GhaffarianHoseini A, Makaremi N, Ghaffarian Hoseini M. Sustainable energy performances of green buildings: A review of current theories, implementations and challenges. Renew Sustain Energy Rev 2013;25:1–17. doi:10.1016/j.rser.2013.01.010.

[2] Gkanas EI, Steriotis TA, Stubos AK, Myler P, Makridis SS. A complete transport validated model on a zeolite membrane for carbon dioxide permeance and capture. Appl Therm Eng 2015; 74:36–46. doi:10.1016/j.applthermaleng.2014.02.006.

[3] Markovska N, Duić N, Mathiesen BV, Guzović Z, Piacentino A, Schlör H, et al. Addressing the main challenges of energy security in the twenty-first century – Contributions of the conferences on Sustainable Development of Energy, Water and Environment Systems. Energy 2016. doi:10.1016/j.energy.2016.10.086.

[4] Lund H, Østergaard PA, Connolly D, Vad Mathiesen B. Smart energy and smart energy systems 2017. doi:10.1016/j.energy.2017.05.123.

[5] Esen M. Thermal performance of a solar-aided latent heat store used for space heating by heat pump. Sol Energy 2000; 69:15–25. doi:10.1016/S0038-092X(00)00015-3.

[6] Paskevicius M, Sheppard DA, Williamson K, Buckley CE. Metal hydride thermal heat storage prototype for concentrating solar thermal power. Energy 2015. doi:10.1016/j.energy.2015.05.068.

[7] Deng S, Wang RZ, Dai YJ. How to evaluate performance of net zero energy building e A literature research. Energy 2014;71:1–16. doi:10.1016/j.energy.2014.05.007.

[8] Marino C, Nucara A, Pietrafesa M, Pudano A. An energy self-sufficient public building using integrated renewable sources and hydrogen storage. Energy 2013. doi:10.1016/j.energy.2013.01.053.

[9] Ghaffarian Hoseini A, Ibrahim R, Baharuddin MN, Ghaffarian Hoseini A. Creating green culturally responsive intelligent buildings: Socio-cultural and environmental influences. Intell Build Int 2011; 3:5–23. doi:10.3763/inbi.2010.0002.

[10] Levin H, Systematic Evaluation and Assessment of Building Environmental Performance (SEABEP), paper for presentation to ``Buildings and Environment'', Paris,9–12June,1997(http://www.wbdg.org/resources/env_sustainability. php?r=envelope),1997.

[11] Hvelplund F. Renewable energy and the need for local energy markets. Energy 2006. doi:10.1016/j.energy.2006.01.016.

[12] Lund H. The implementation of renewable energy systems. Lessons learned from the Danish case. Energy 2010. doi:10.1016/j.energy.2010.01.036.

[13] Juan Y-K, Gao P, Wang J. A hybrid decision support system for sustainable office building renovation and energy performance improvement. Energy Build 2010;42:290–7. doi:10.1016/j.enbuild.2009.09.006.

[14] Bland A, Khzouz M, Statheros T, Gkanas EI. PCMs for Residential Building Applications: A Short Review Focused on Disadvantages and Proposals for Future Development. Buildings 2017;7.

[15] Dagdougui H, Minciardi R, Ouammi A, Robba M, Sacile R. Modeling and optimization of a hybrid system for the energy supply of a “Green” building. Energy Convers Manag 2012;64:351–63. doi:10.1016/j.enconman.2012.05.017.

[16] Verbecke F, Vesy B. Safety strategy for the first deployment of a hydrogen-based green public building in France. Int J Hydrogen Energy 2013;38:8053–60. doi:10.1016/j.ijhydene.2013.03.019.

[17] Mancarella P. MES (multi-energy systems): An overview of concepts and evaluation models. Energy 2014. doi:10.1016/j.energy.2013.10.041.

[18] Carton JG, Olabi AG. Design of experiment study of the parameters that affect performance of three flow plate configurations of a proton exchange membrane fuel cell. Energy 2010;35:2796–806. doi:10.1016/j.energy.2010.02.044.

[19] Principi G, Agresti F, Maddalena A, Lo Russo S. The problem of solid state hydrogen storage. Energy 2009. doi:10.1016/j.energy.2008.08.027.

[20] Komiyama R, Otsuki T, Fujii Y. Energy modeling and analysis for optimal grid integration of large-scale variable renewables using hydrogen storage in Japan. Energy 2015. doi:10.1016/j.energy.2014.12.069.

[21] Madaria Y, Anil Kumar E. Effect of heat transfer enhancement on the performance of metal hydride based hydrogen compressor. Int J Hydrogen Energy 2016;41:3961–73. doi:10.1016/j.ijhydene.2016.01.011.

[22] Gkanas EI, Khzouz M. Numerical analysis of candidate materials for multi-stage metal hydride hydrogen compression processes. Renew Energy 2017;111:484–93. doi:10.1016/j.renene.2017.04.037.

[23] Wenelska K, Michalkiewicz B, Chen X, Mijowska E. Pd nanoparticles with tunable diameter deposited on carbon nanotubes with enhanced hydrogen storage capacity. Energy 2014;75:549–54. doi:10.1016/J.ENERGY.2014.08.016.

[24] Schlapbach L, Zuttel A. Hydrogen-storage materials for mobile applications. Nature 2001;414:353–8.

[25] Ni J, Liu H. Experimental research on refrigeration characteristics of a metal hydride heat pump in auto air-conditioning. Int J Hydrogen Energy 2007;32:2567–72. doi:10.1016/j.ijhydene.2006.09.038.

[26] Gkanas EI, Makridis SS, Stubos AK. Modeling and simulation for absorption-desorption cyclic process on a three-stage metal hydride hydrogen compressor. Computer Aided Chem Engineering 2013;32:379-384. doi:10.1016/B978-0-444-63234-0.50064-6.

[27] Muthukumar P, Singh Patel K, Sachan P, Singhal N. Computational study on metal hydride based three-stage hydrogen compressor. Int J Hydrogen Energy 2012;37:3797–806. doi:10.1016/j.ijhydene.2011.05.104.

[28] Koultoukis ED, Gkanas EI, Makridis SS, Christodoulou CN, Fruchart D, Stubos AK. High-temperature activated AB2 nanopowders for metal hydride hydrogen compression. Int J Energy Res 2014;38. doi:10.1002/er.3147.

[29] Gkanas EI, Grant DM, Khzouz M, Stuart AD, Manickam K, Walker GS. Efficient hydrogen storage in up-scale metal hydride tanks as possible metal hydride compression agents equipped with aluminium extended surfaces. Int J Hydrogen Energy 2016;41. doi:10.1016/j.ijhydene.2016.04.035.

[30] Talagañis BA, Meyer GO, Aguirre PA. Modeling and simulation of absorption–desorption cyclic processes for hydrogen storage-compression using metal hydrides. Int J Hydrogen Energy 2011;36:13621–31. doi:10.1016/j.ijhydene.2011.07.139.

[31] Talagañis BA, Meyer GO, Oliva DG, Fuentes M, Aguirre PA. Modeling and optimal design of cyclic processes for hydrogen purification using hydride-forming metals. Int J Hydrogen Energy 2014;39:18997–9008. doi:10.1016/j.ijhydene.2014.09.045.

[32] Yang FS, Zhang ZX, Wang GX, Bao ZW, Diniz da Costa JC, Rudolph V. Numerical study of a metal hydride heat transformer for low-grade heat recovery. Appl Therm Eng 2011;31:2749–56. doi:10.1016/j.applthermaleng.2011.04.047.

[33] Sajid Ahmed S, Srinivasa Murthy S. Analysis of a novel metal hydride cycle for simultaneous heating and cooling. Renew Energy 2004;29:615–31. doi:10.1016/j.renene.2003.07.005.

[34] Anbarasu S, Muthukumar P, Mishra SC. Thermal modeling of LmNi4.91Sn0.15 based solid state hydrogen storage device with embedded cooling tubes. Int J Hydrogen Energy 2014;39:15549–62. doi:10.1016/j.ijhydene.2014.07.088.

[35] Mazzucco A, Dornheim M, Sloth M, Jensen TR, Jensen JO, Rokni M. Bed geometries, fueling strategies and optimization of heat exchanger designs in metal hydride storage systems for automotive applications: A review. Int J Hydrogen Energy 2014;39:17054–74. doi:10.1016/j.ijhydene.2014.08.047.

[36] Gkanas EI, Makridis SS. Effective thermal management of a cylindrical MgH2 tank including thermal coupling with an operating SOFC and the usage of extended surfaces during the dehydrogenation process. Int J Hydrogen Energy 2016;41:5693–708. doi:10.1016/j.ijhydene.2016.01.165.

[37] Gkanas EI, Grant DM, Stuart AD, Eastwick CN, Book D, Nayebossadri S, et al. Numerical study on a two-stage Metal Hydride Hydrogen Compression system. J Alloys Compd 2015;645:S18–22. doi:10.1016/j.jallcom.2015.03.123.

[38] Makridis SS, Gkanas EI, Panagakos G, Kikkinides ES, Stubos AK, Wagener P, et al. Polymer-stable magnesium nanocomposites prepared by laser ablation for efficient hydrogen storage. Int J Hydrogen Energy 2013;38. doi:10.1016/j.ijhydene.2013.04.031.

[39] Jemni A. Study of two-dimensional heat and mass transfer during absorption in a metal-hydrogen reactor. Int J Hydrogen Energy 1995;20:43–52. doi:10.1016/0360-3199(93)E0007-8.

[40] Visaria M, Mudawar I, Pourpoint T, Kumar S. Study of heat transfer and kinetics parameters influencing the design of heat exchangers for hydrogen storage in high-pressure metal hydrides. Int J Heat Mass Transf 2010;53:2229–39. doi:10.1016/j.ijheatmasstransfer.2009.12.010.

[41] Ha MY, Kim IK, Song HD, Sung S, Lee DH. A numerical study of thermo-fluid phenomena in metal hydride beds in the hydriding process. Int J Heat Mass Transf 2004;47:2901–12. doi:10.1016/j.ijheatmasstransfer.2004.03.014.

[42] Laurencelle F, Goyette J. Simulation of heat transfer in a metal hydride reactor with aluminium foam. Int J Hydrogen Energy 2007;32:2957–64. doi:10.1016/j.ijhydene.2006.12.007.

[43] Raju M, Ortmann JP, Kumar S. System simulation model for high-pressure metal hydride hydrogen storage systems. Int J Hydrogen Energy 2010;35:8742–54. doi:10.1016/j.ijhydene.2010.05.024.

[44] Kim KJ, Montoya B, Razani A, Lee K-H. Metal hydride compacts of improved thermal conductivity. Int J Hydrogen Energy 2001;26:609–13. doi:10.1016/S0360-3199(00)00115-4.

[45] Rodriguez Sanchez A, Klein HP, Groll M. Expanded graphite as heat transfer matrix in metal hydride beds. Int J Hydrogen Energy 2003;28:515–27. doi:10.1016/S0360-3199(02)00057-5.

[46] Melnichuk M, Silin N. Guidelines for thermal management design of hydride containers. Int J Hydrogen Energy 2012;37:18080–94. doi:10.1016/j.ijhydene.2012.09.046.

[47] Gambini M, Stilo T, Vellini M, Montanari R. High temperature metal hydrides for energy systems Part A: Numerical model validation and calibration. Int J Hydrogen Energy 2017;42:16195–202. doi:10.1016/j.ijhydene.2017.05.062.

[48] Busqué R, Torres R, Grau J, Roda V, Husar A. Effect of metal hydride properties in hydrogen absorption through 2D-axisymmetric modeling and experimental testing in storage canisters. Int J Hydrogen Energy 2017;42:19114–25. doi:10.1016/j.ijhydene.2017.06.125.

[49] Muthukumar P, Satheesh A, Linder M, Mertz R, Groll M. Studies on hydriding kinetics of some La-based metal hydride alloys. Int J Hydrogen Energy 2009;34:7253–62. doi:10.1016/j.ijhydene.2009.06.075.

[50] Muthukumar P, Linder M, Mertz R, Laurien E. Measurement of thermodynamic properties of some hydrogen absorbing alloys. Int J Hydrogen Energy 2009;34:1873–9. doi:10.1016/j.ijhydene.2008.12.052.

[51] Nishizaki T, Miyamoto K, Yoshida K. Coefficients of performance of hydride heat pumps. J Less Common Met 1983;89:559–66. doi:10.1016/0022-5088(83)90372-7.

[52] Bowman RC, Luo CH, Ahn CC, Witham CK, Fultz B. The effect of tin on the degradation of LaNi5−ySny metal hydrides during thermal cycling. J Alloys Compd 1995;217:185–92. doi:10.1016/0925-8388(94)01337-3.

[53] Muthukumar P, Singhal A, Bansal GK. Thermal modeling and performance analysis of industrial-scale metal hydride based hydrogen storage container. Int J Hydrogen Energy 2012;37:14351–64. doi:10.1016/j.ijhydene.2012.07.010.

Table 1. Control factors used for the optimization process

	L (mm)	h_t (W/m^{2}K)	Number of Tubes
Geometry 1	*14.39/12.11/10.39/9.01/7.89*	*200/500/1000/2000/5000*	*8/9/10/11/12*
Geometry 2	*14.39/12.11/10.39/9.01/7.89*	*200/500/1000/2000/5000*	*16/18/20/22/24*
Geometry 3	*14.39/12.11/10.39/9.01/7.89*	*200/500/1000/2000/5000*	*12/13/15/16/18*

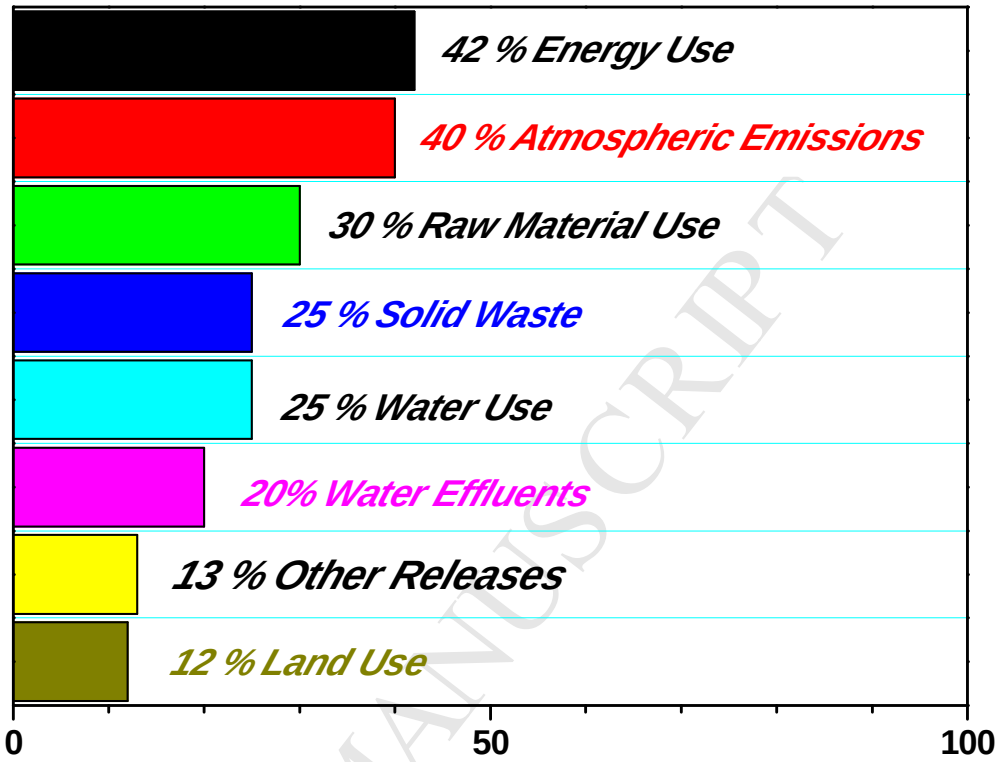

Figure 1. Environmental impact of buildings [10]

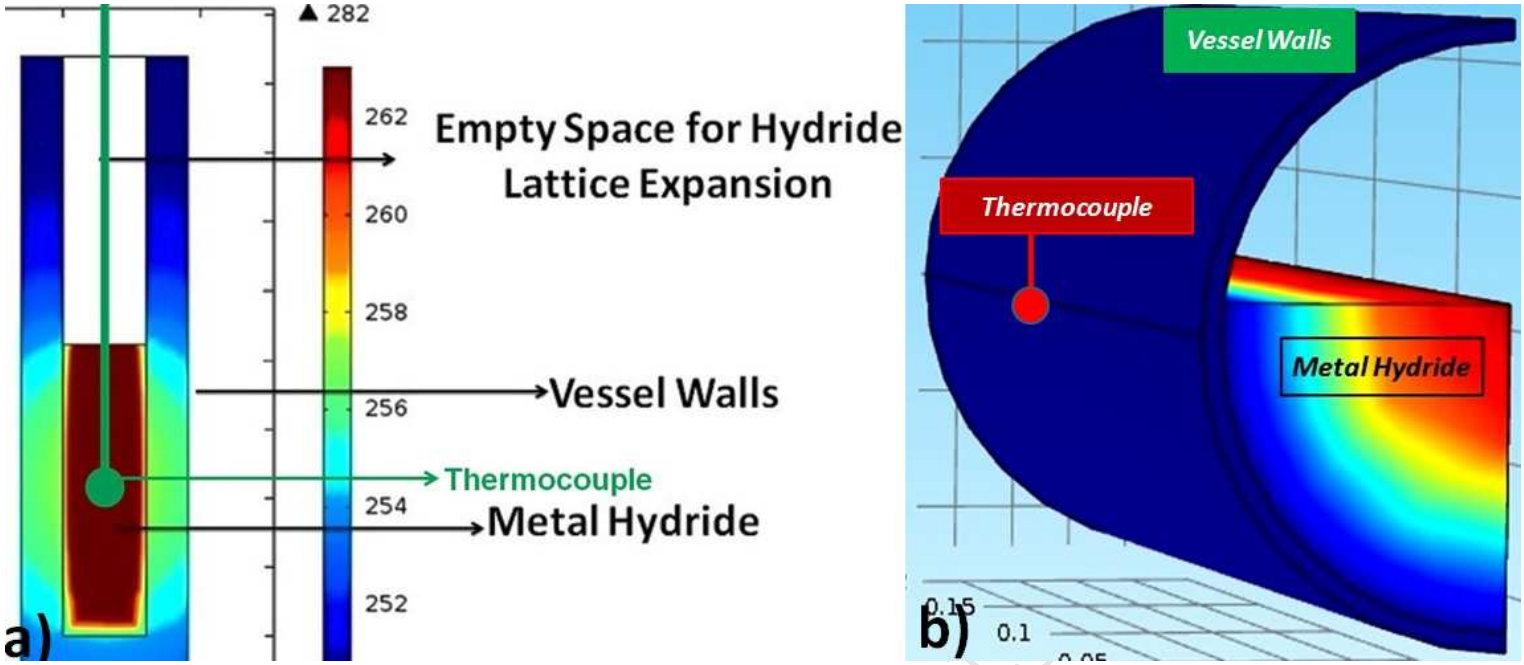

Figure 2. Geometries used for the validation of the numerical model. Figure 2a shows the geometry used for the validation of $LaNi_5$ and the position of the thermocouple and Figure 2b shows the geometry used for the validation of the AB_2-intermetallic.

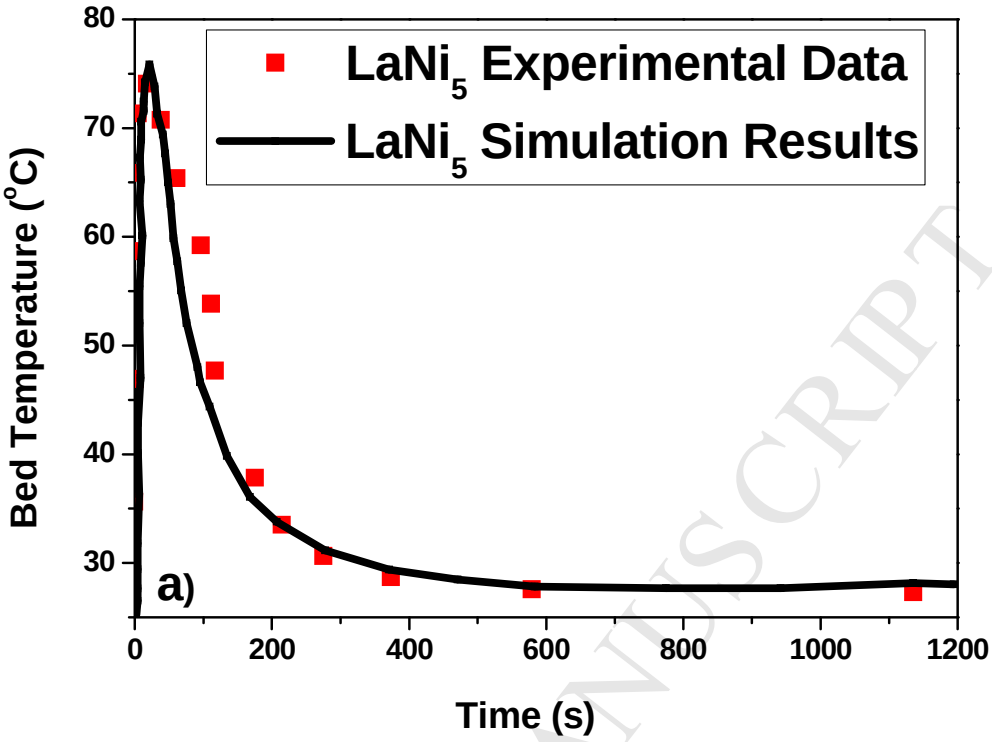

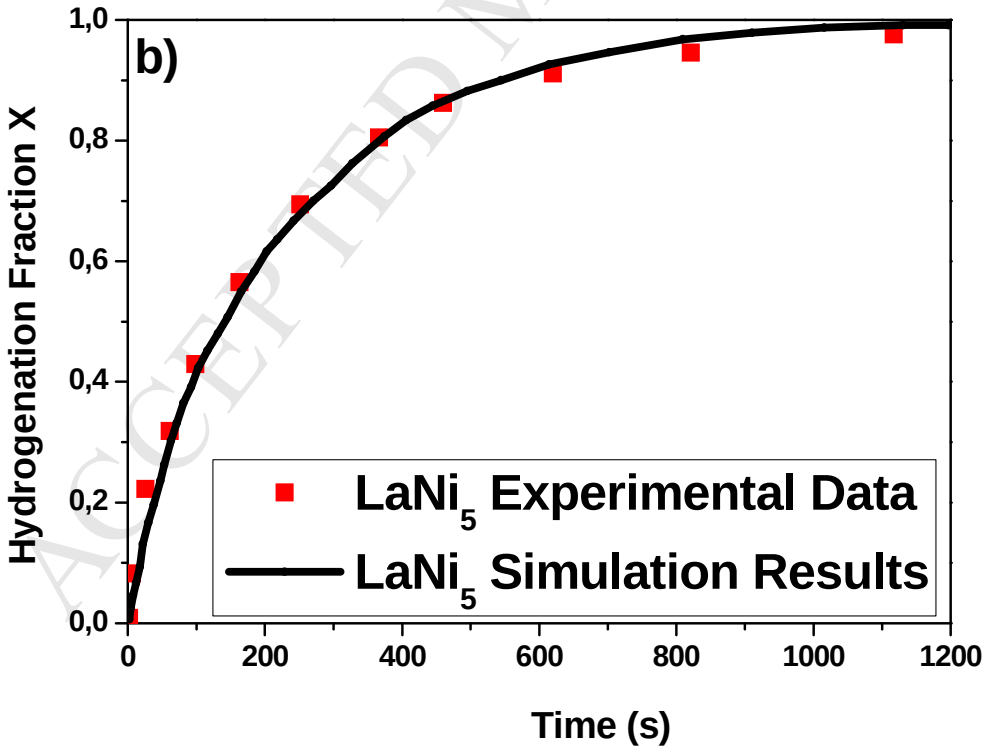

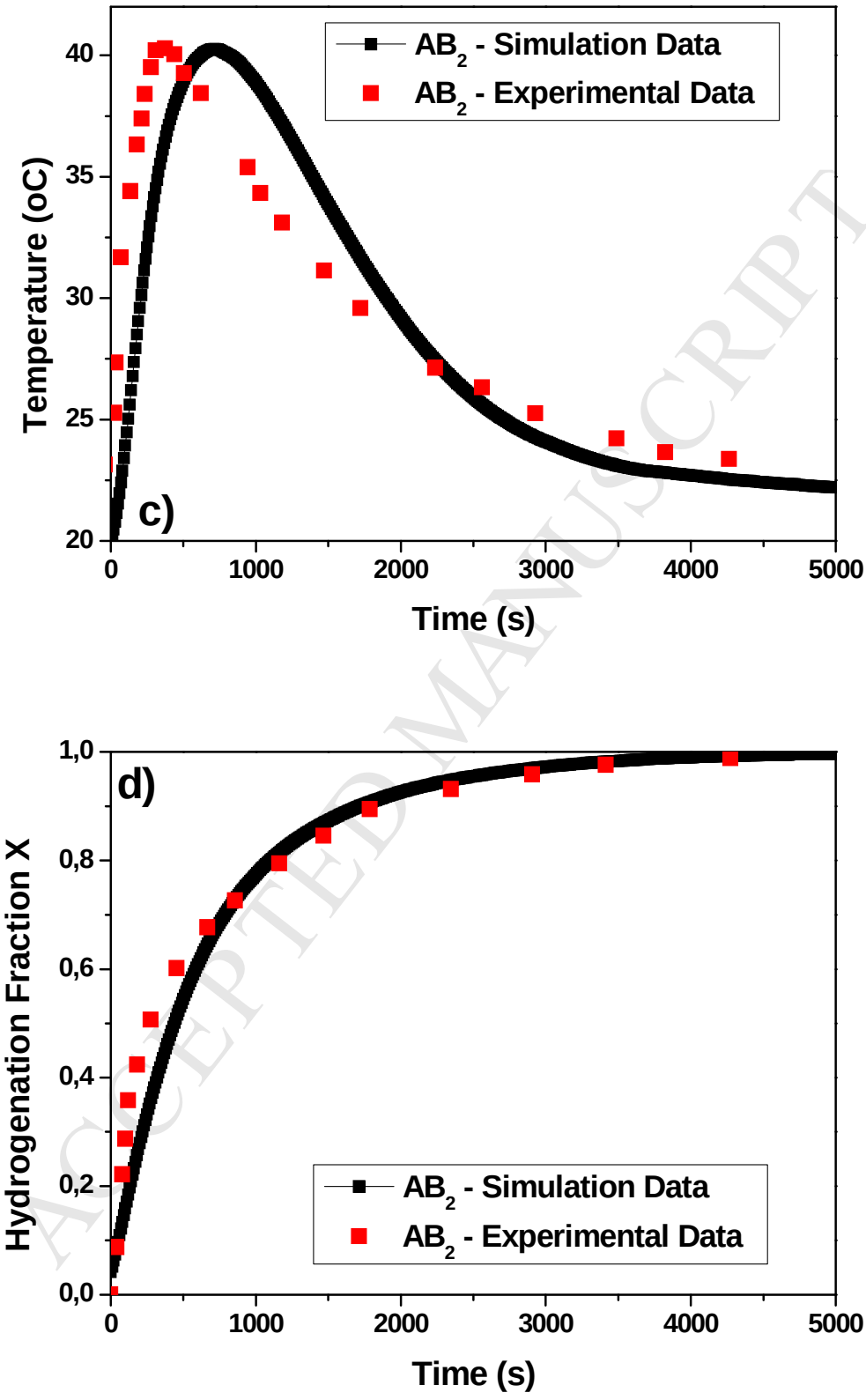

Figure 3. Validation of the predicted amount of hydrogen stored (3a) for different temperatures and different pressures and released (3b) for two different temperatures with experimental data extracted from a lab scale Sievert type apparatus. Fig 1c shows the validation of the temperature profile of the AB2-intermetallic and Fig. 1d presents the validation of the hydrogenation behavior of the same

material. The experimental results (dots) with the simulation results (lines) are in good agreement with a maximum deviation less than 5%.

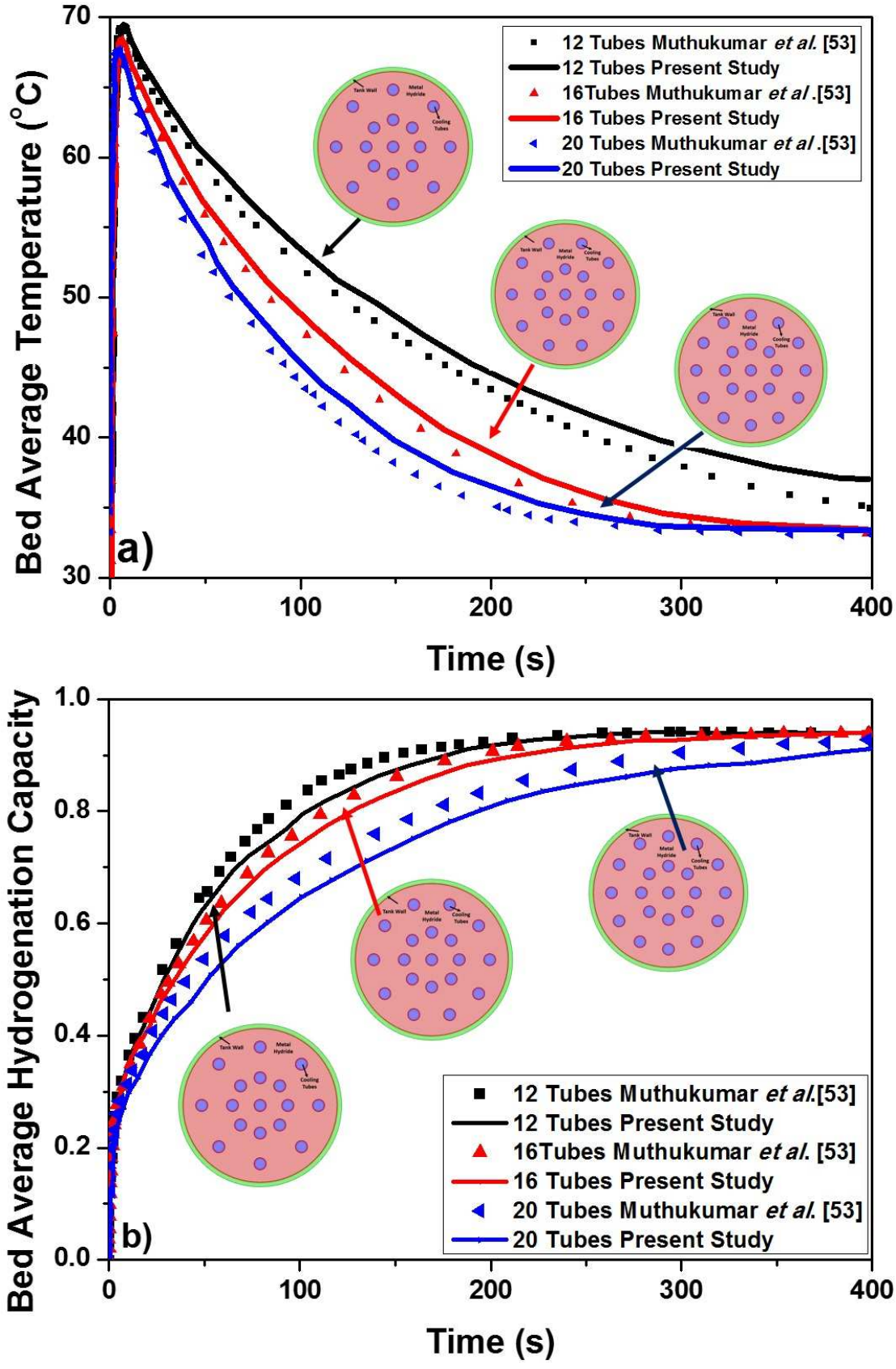

Figure 4. Validation of the proposed numerical model regarding the ability to predict the convective heat transfer with the results published by Muthukumar et al. [53]. Figure 4a presents the comparison

of the average bed temperature and Figure 4b presents the comparison of the average hydrogenation capacity

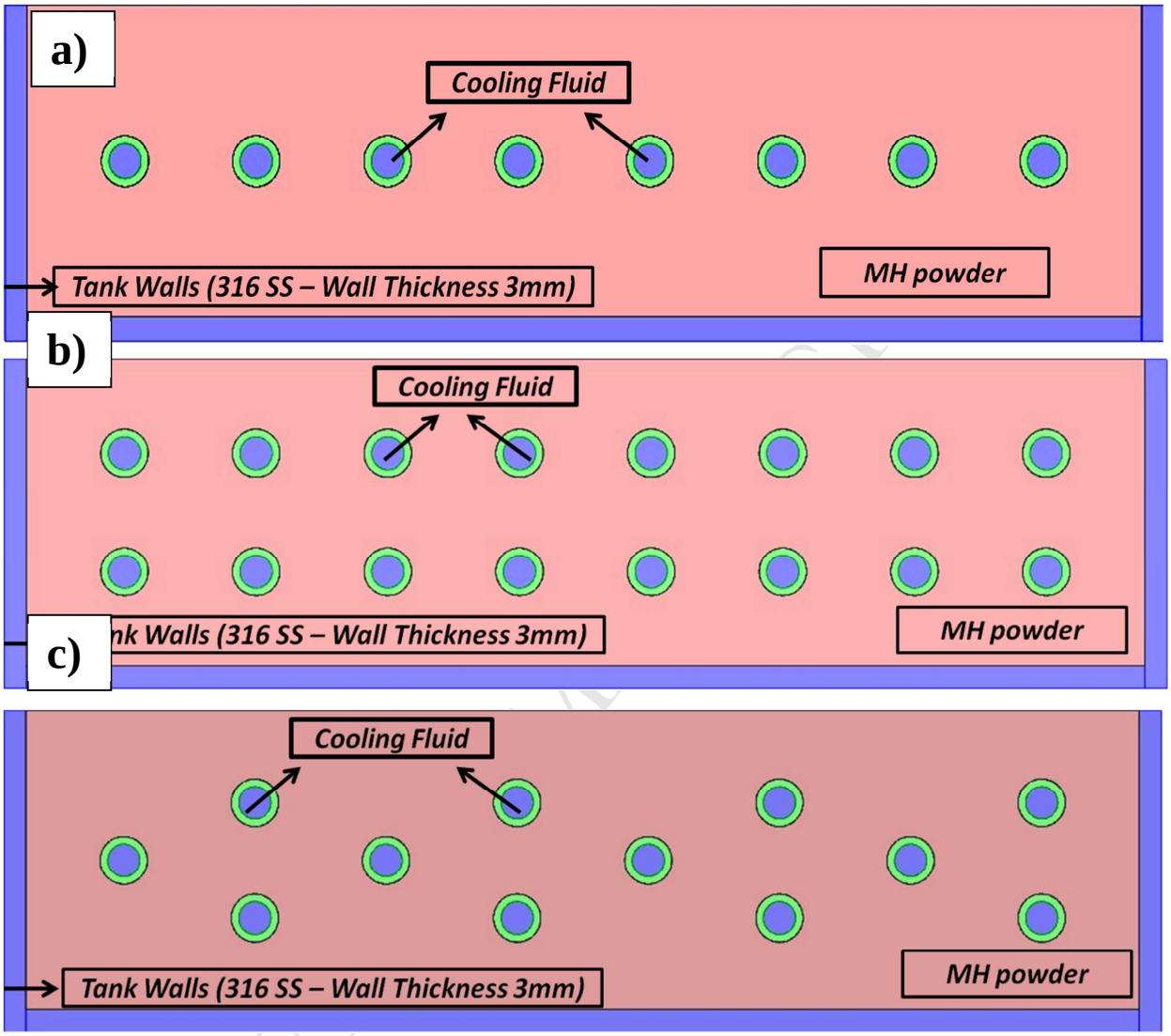

Figure 5. Cross-section of the three heat management geometries. Figure 5a shows the first geometry with a single row of tubes (Geometry 1). Figure 5b presents the second geometry with double row of cooling tubes (Geometry 2) and Figure 5c shows the third geometry (Geometry 3) with a mixed tube arrangement.

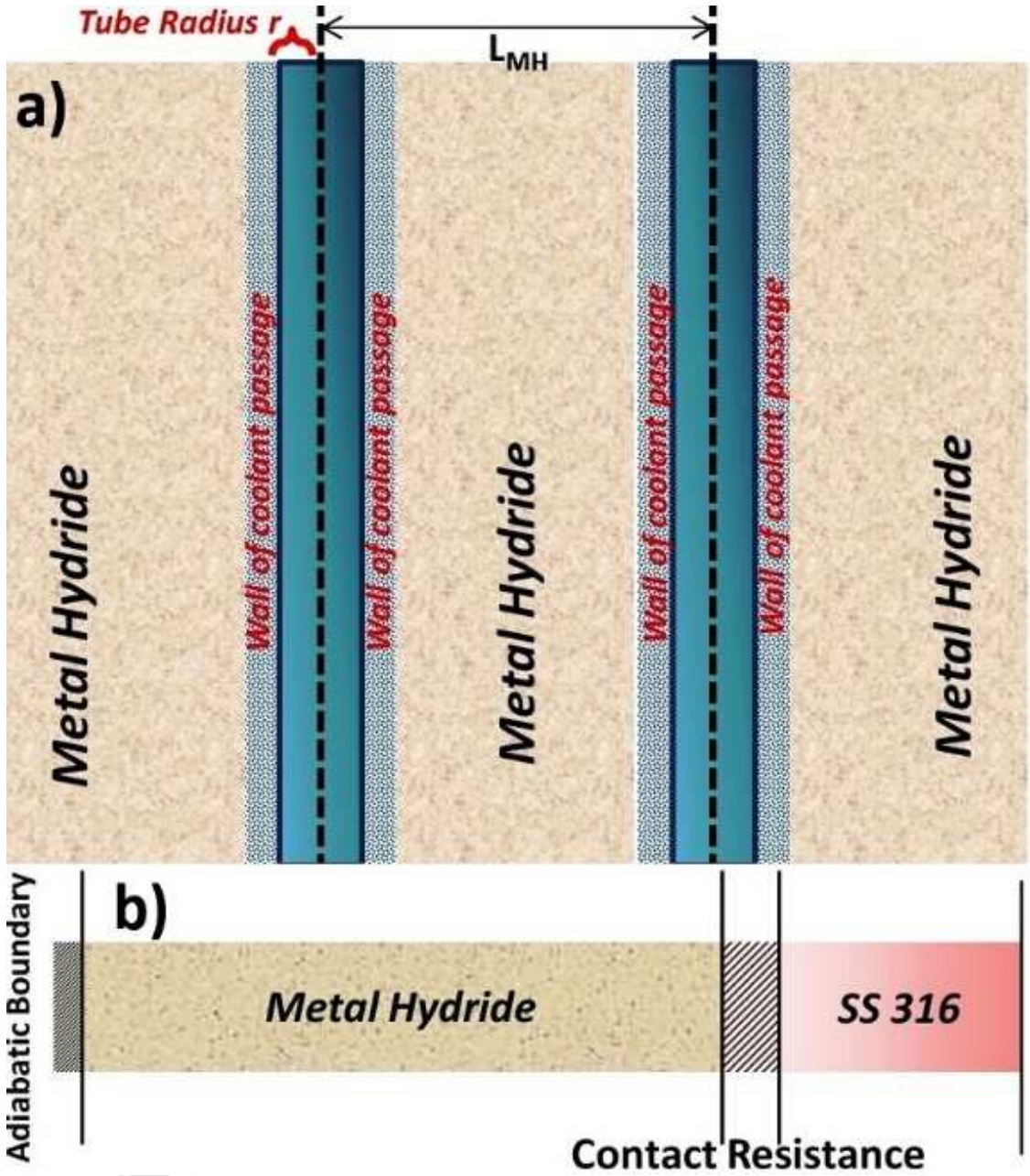

Figure. 6 Definition of the metal hydride thickness. Figure 6a shows the metal hydride thickness defined as the distance between the centres of two adjacent tubes. Figure 6b shows that the metal hydride thickness consists of the tube wall, the contact resistance and the metal hydride.

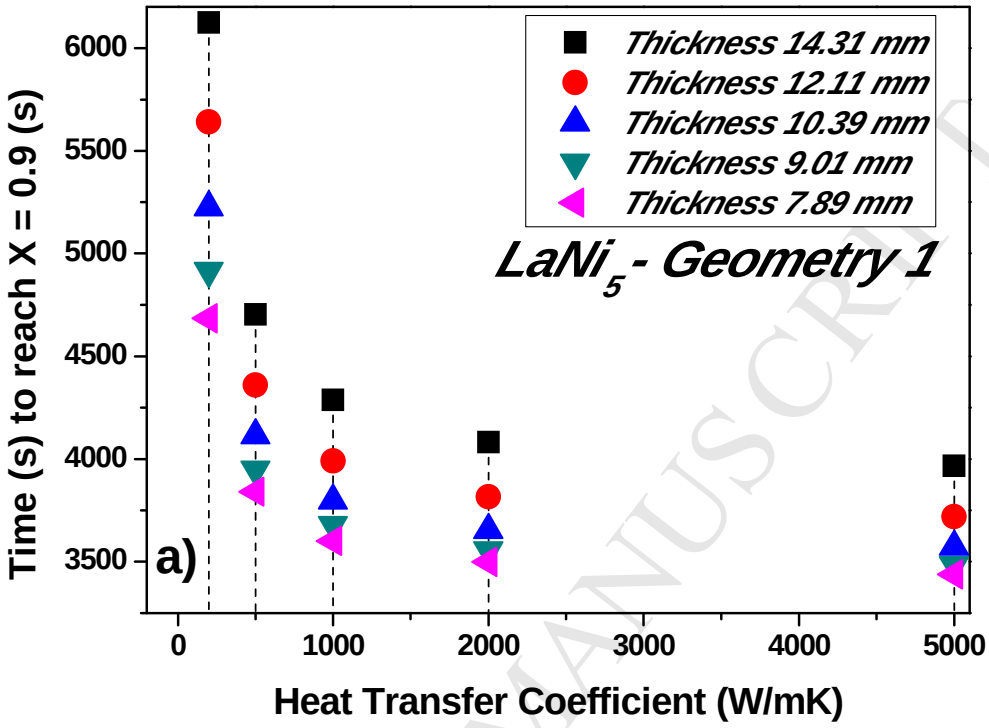

Figure 7. Hydrogenation response of $LaNi_5$ when using Geometry 1 for the heat management process, for all the different metal hydride thicknesses and all the values of the heat transfer coefficient.

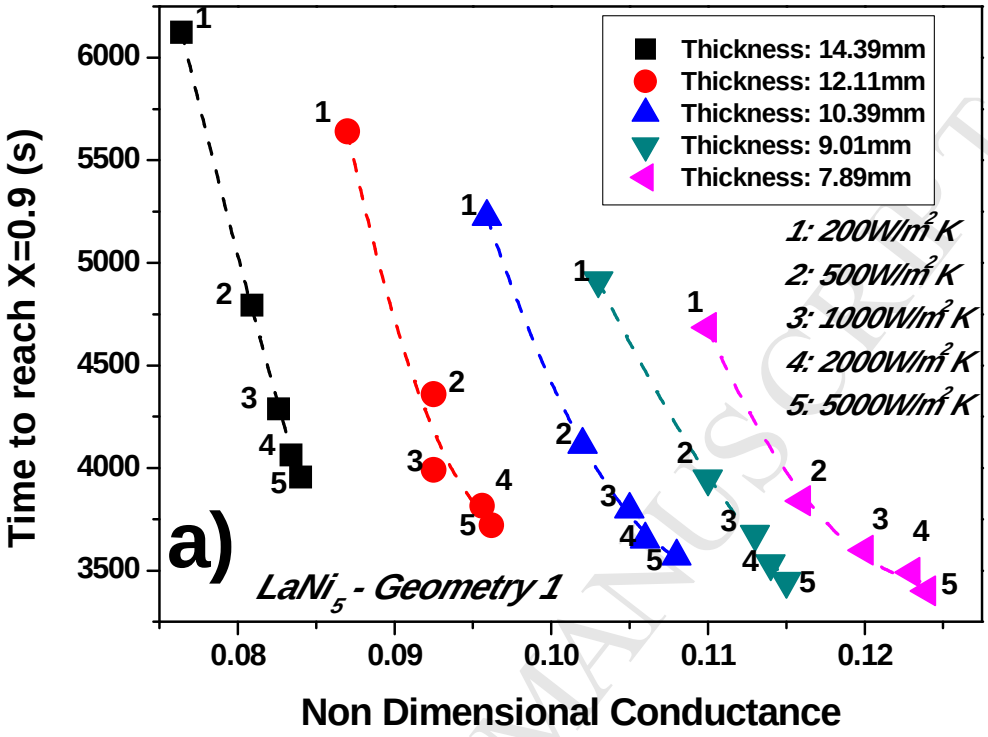
Thickness: 14.39mm
Thickness: 12.11mm
Thickness: 10.39mm
Thickness: 9.01mm
Thickness: 7.89mm
1: 200W/m² K
2: 500W/m² K
3: 1000W/m² K
4: 2000W/m² K
5: 5000W/m² K
a)
LaNi5 - Geometry 1
Time to reach X=0.9 (s)
Non Dimensional Conductance

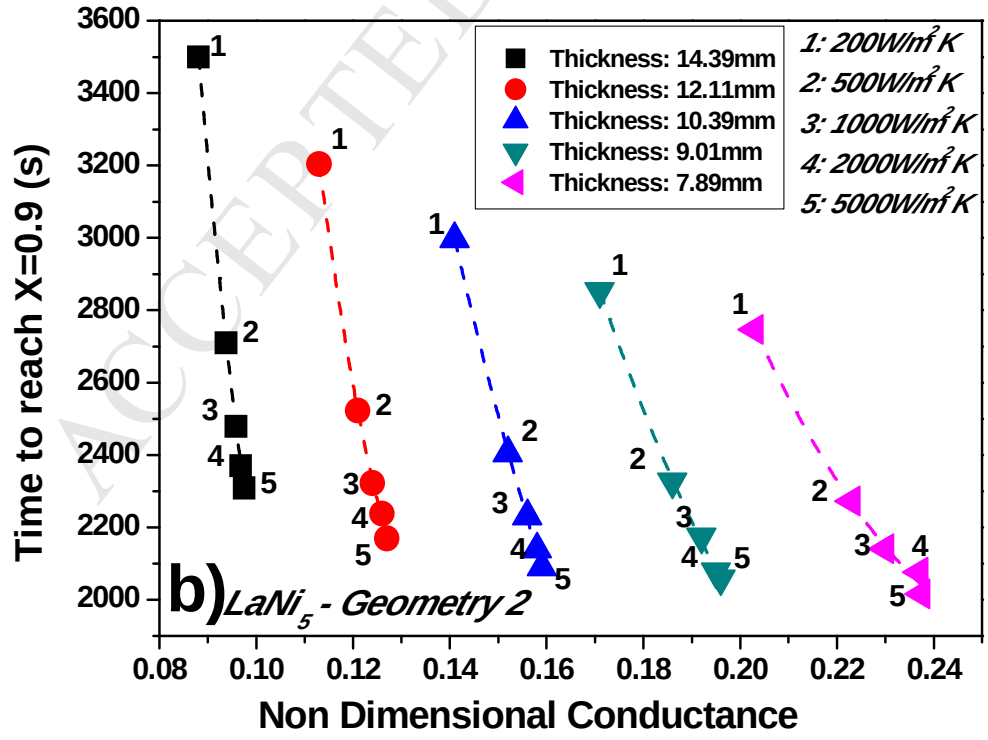
Thickness: 14.39mm
Thickness: 12.11mm
Thickness: 10.39mm
Thickness: 9.01mm
Thickness: 7.89mm
1: 200W/m² K
2: 500W/m² K
3: 1000W/m² K
4: 2000W/m² K
5: 5000W/m² K
b)
LaNi5 - Geometry 2
Time to reach X=0.9 (s)
Non Dimensional Conductance

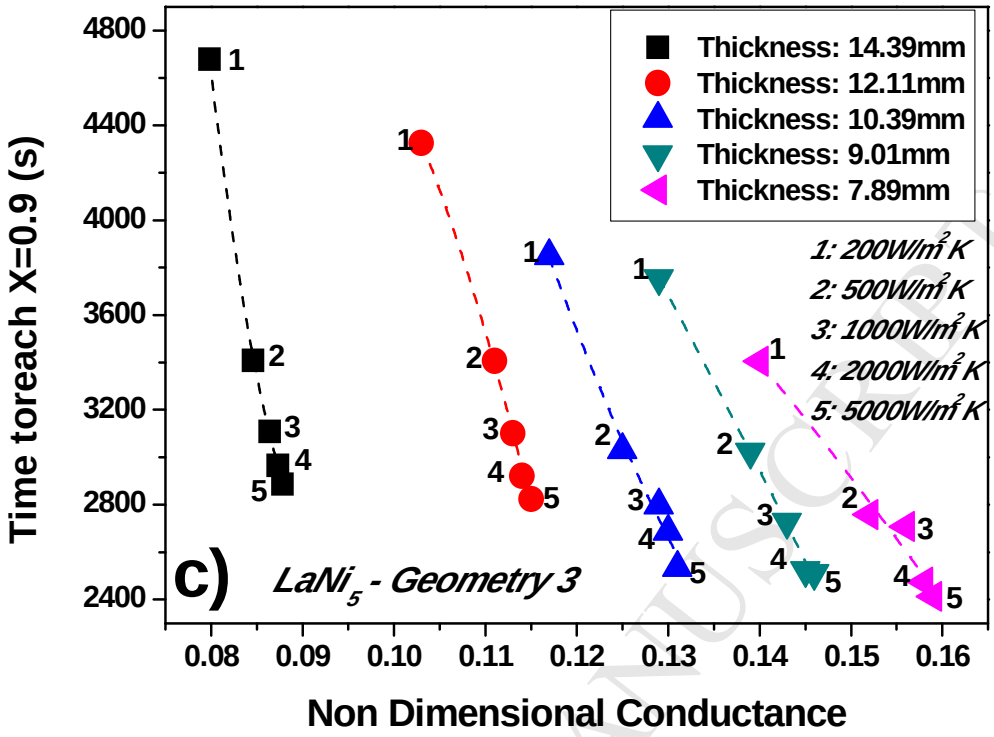

Figure 8. Variation of the charging time with the NDC. Figure 8a shows represents the behavior of Geometry 1, while Figure 8b and 8c shows the behavior of Geometry 2 and 3 respectively.

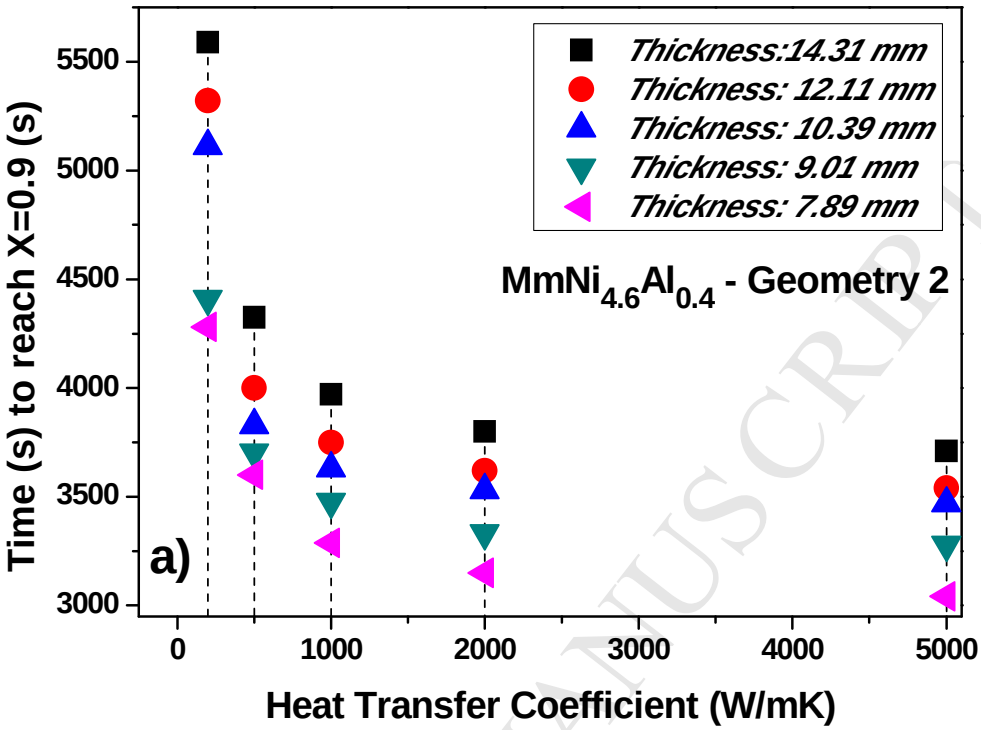

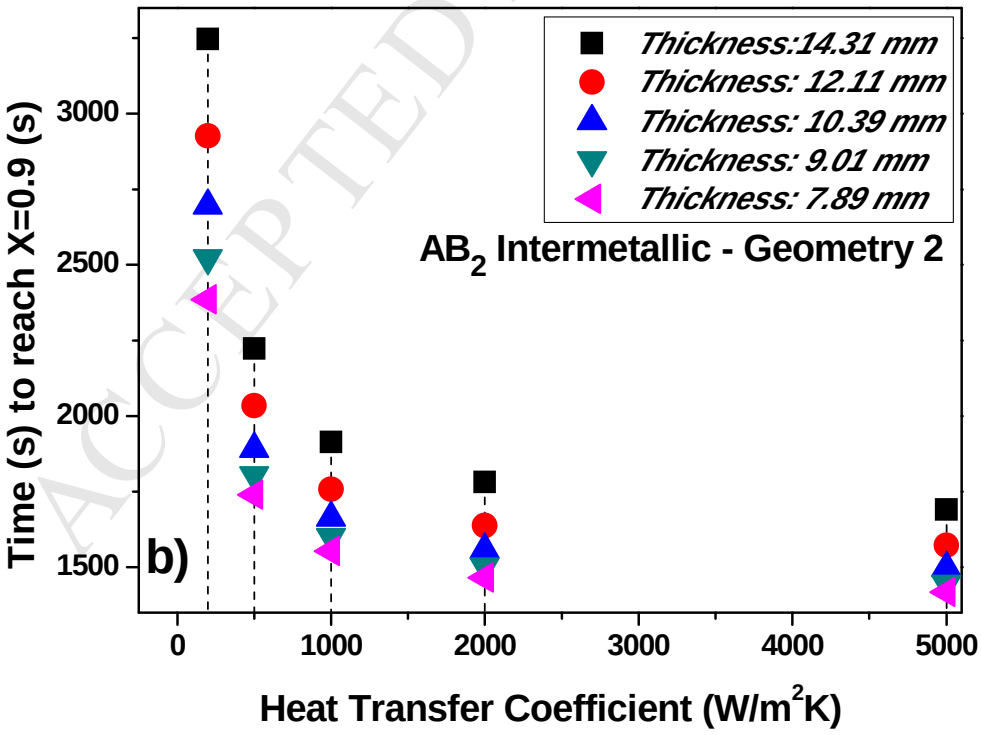

Figure 9. Hydrogenation response of $MmNi_{4.6}Al_{0.4}$ (9a) and the AB_2-intermetallic (9b) when using Geometry 2 for the heat management process, for all the different metal hydride thicknesses and all the values of the heat transfer coefficient.

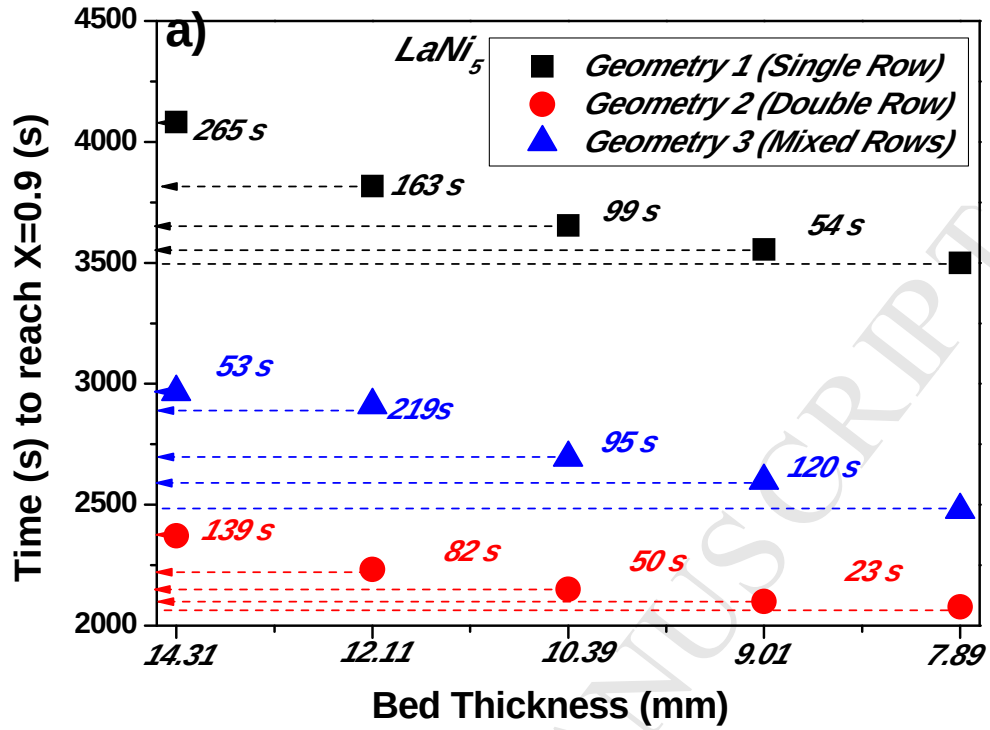

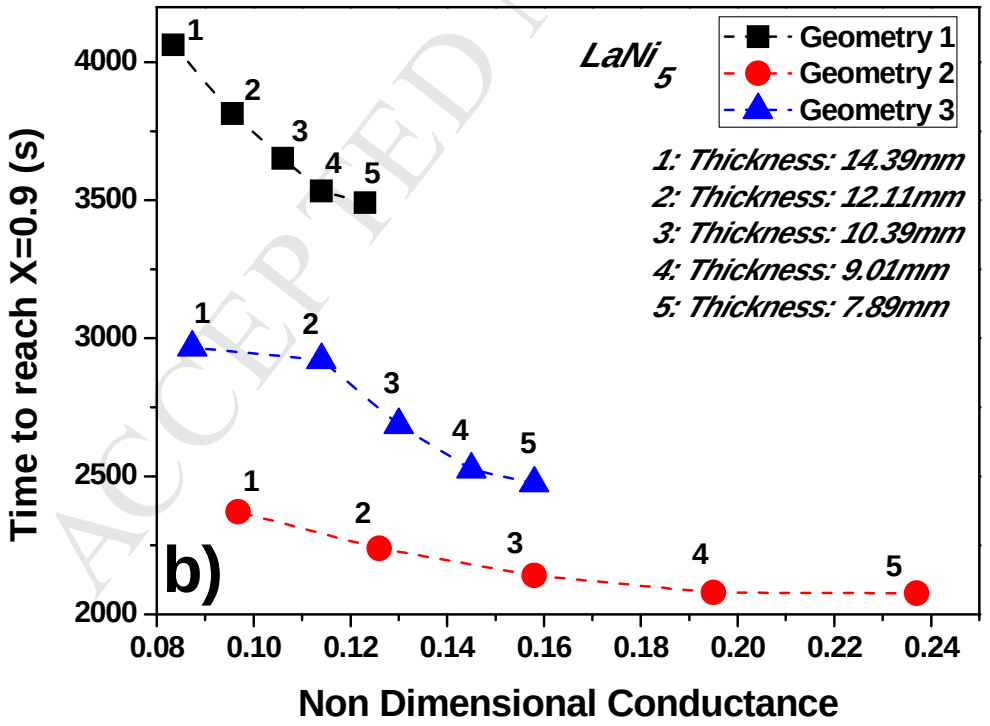

Figure 10. Effect of the metal hydride thickness on the hydrogenation behavior of $LaNi_5$. Figure 10a shows the comparison of the hydrogenation behavior of all the geometries for all the possible metal hydride thicknesses and Figure 10b shows the hydrogenation process with the NDC.

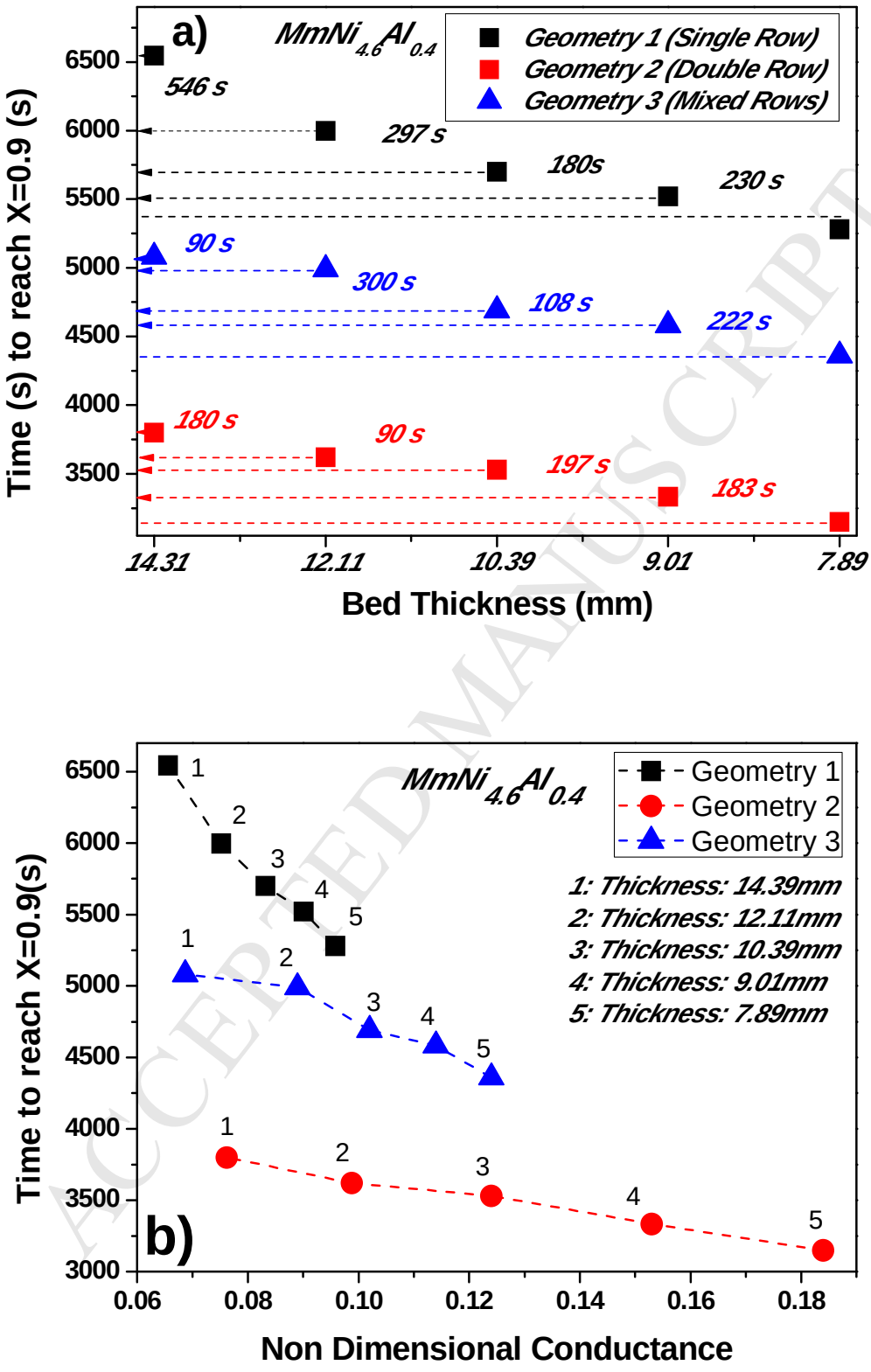

Figure 11. Effect of the metal hydride thickness on the hydrogenation behavior of $MmNi_{4.6}Al_{0.4}$. Figure 11a shows the comparison of the hydrogenation behavior of all the geometries for all the possible metal hydride thicknesses and Figure 11b shows the hydrogenation process with the NDC.

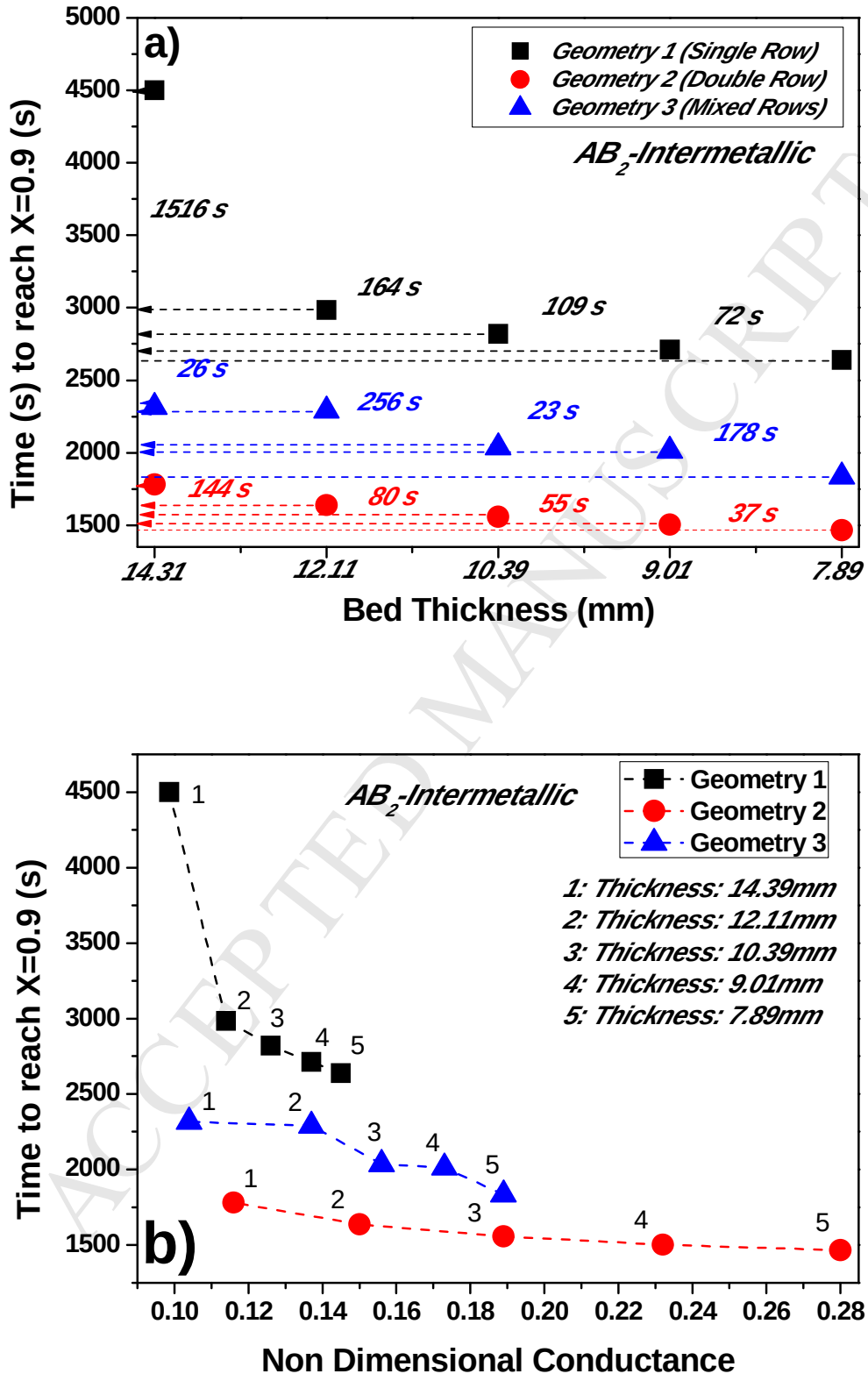

Figure 12. Effect of the metal hydride thickness on the hydrogenation behavior of the AB_2 Intermetallic. Figure 12a shows the comparison of the hydrogenation behavior of all the geometries for

all the possible metal hydride thicknesses and Figure 12b shows the hydrogenation process with the NDC.

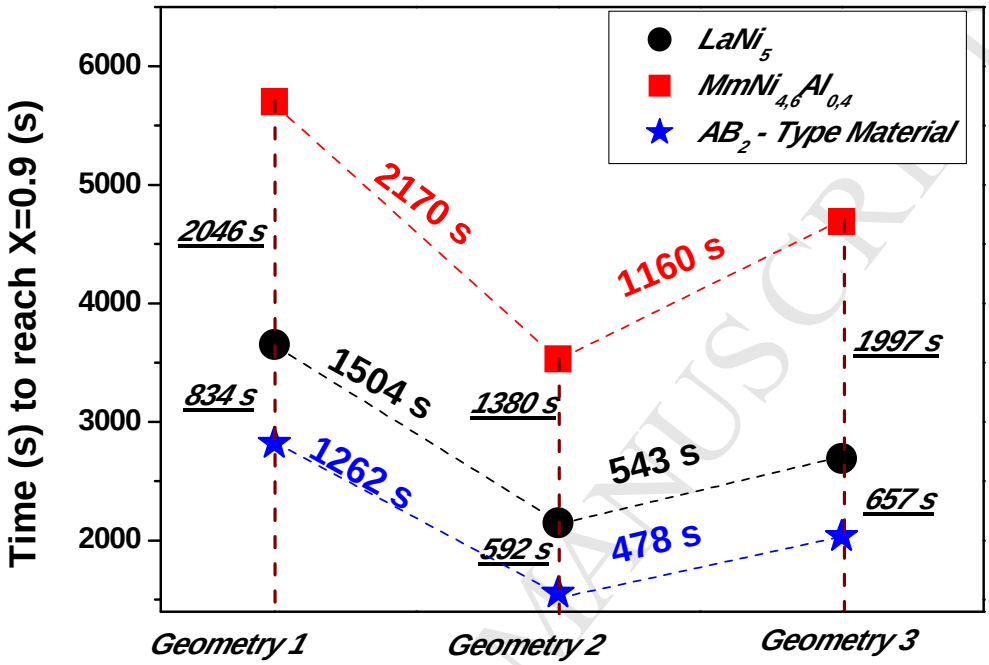

Figure 13. Comparison of the hydrogenation behavior of all the materials and all geometries when using the optimum values of ht=2000[W/m2K] and L=10.39mm

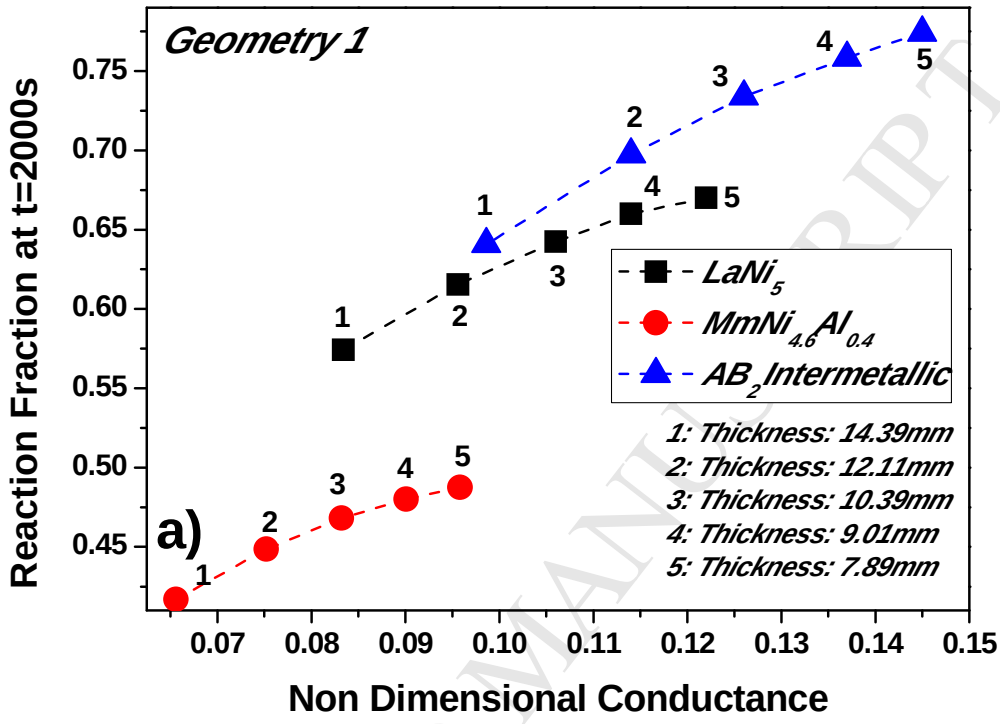

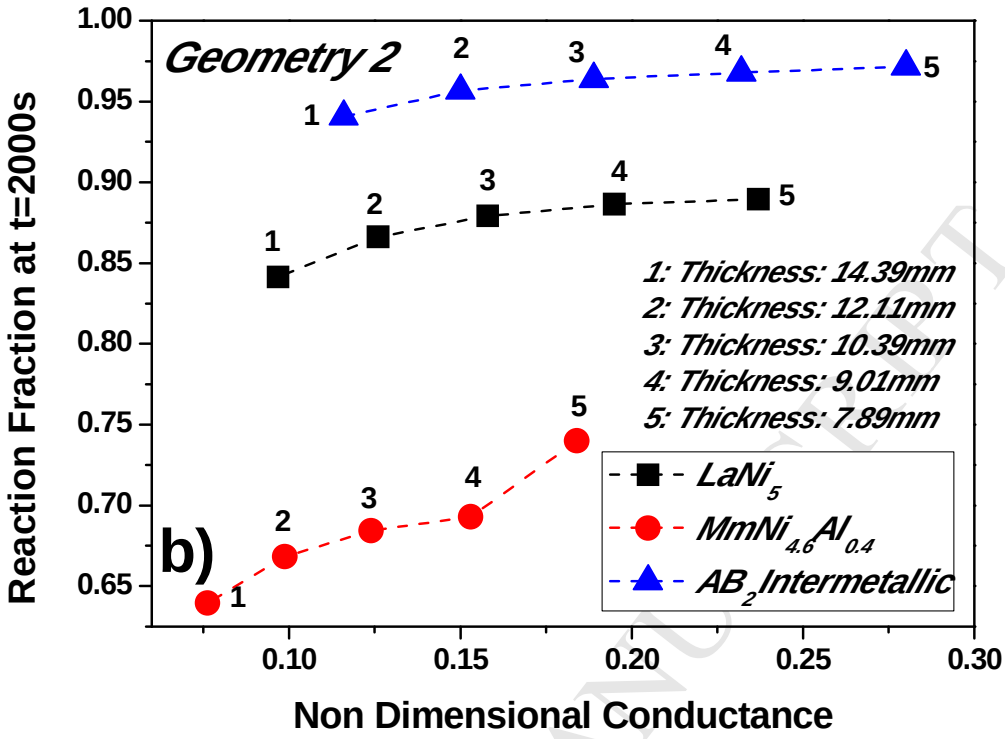

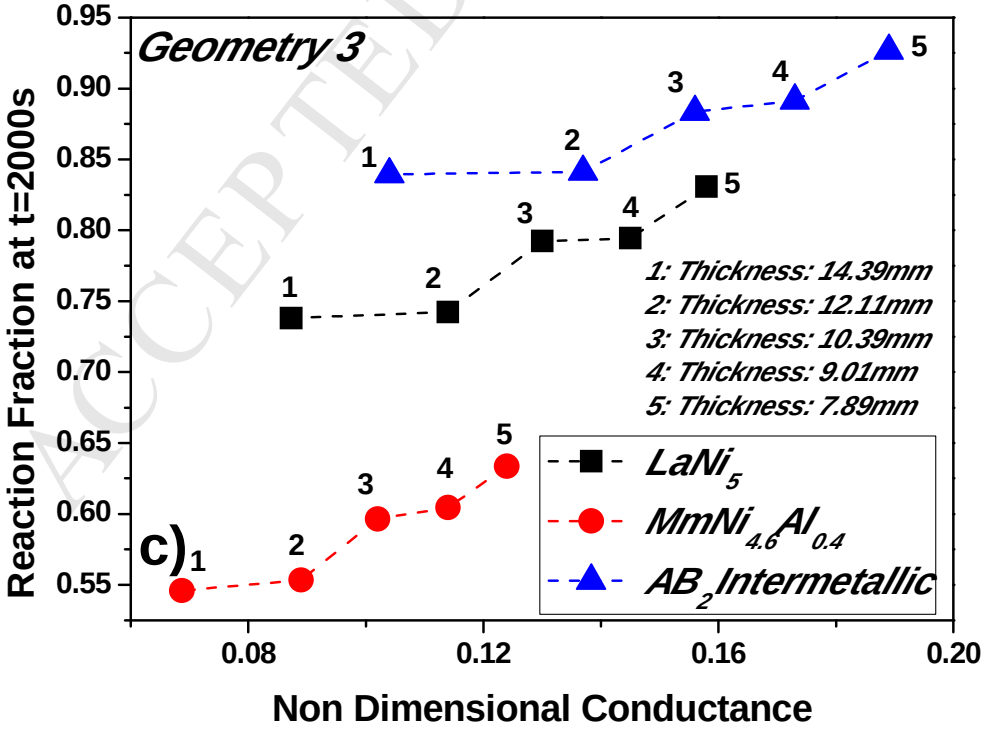

Figure 14. Comparison of the reaction fraction at the end of the desired charging time with the NDC. Figure 14a presents the comparison for Geometry 1, while Figure 14b and 14c for the Geometry 2 and 3 respectively.

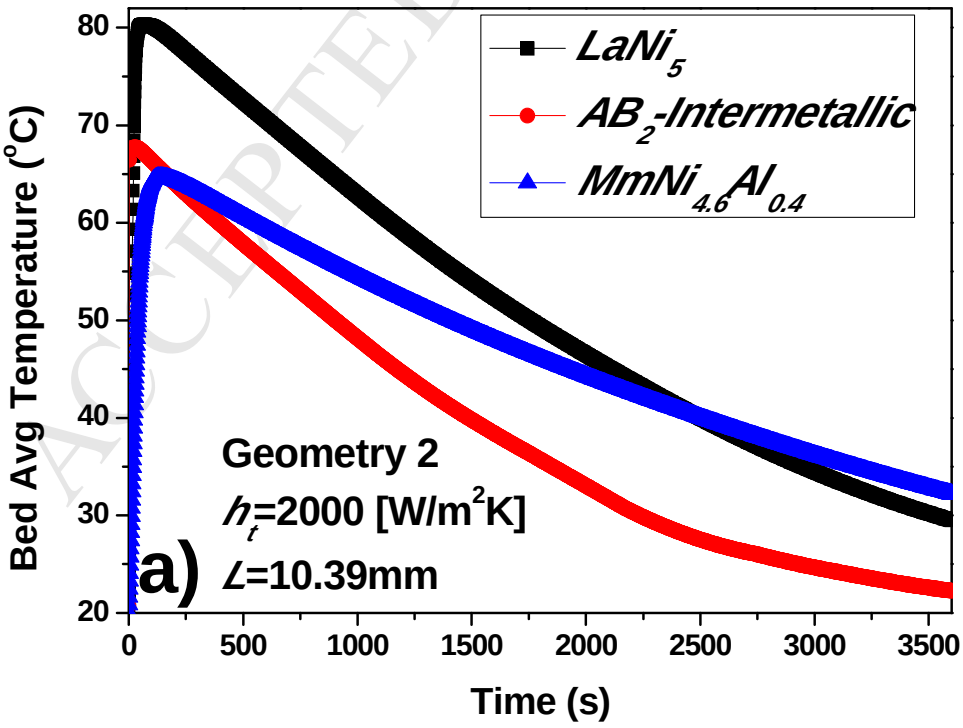

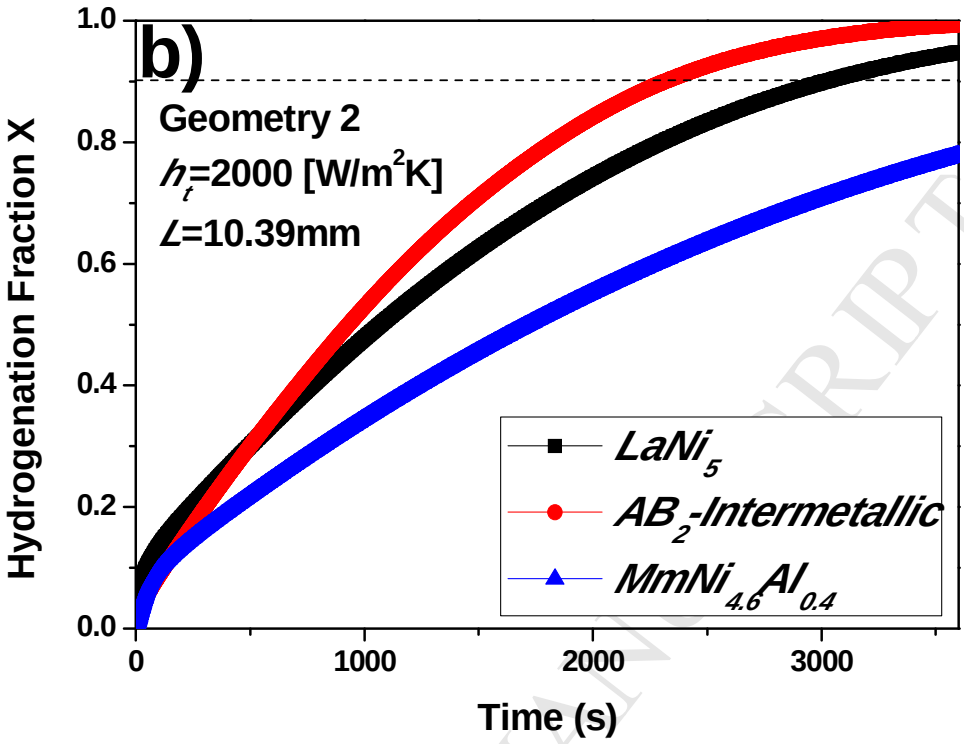

Figure 15. Average temperature evolution (15a) and average hydrogenation fraction evolution (15b) for all the materials when using Geometry 2 and metal hydride thickness of 10.39 mm at a heat transfer coefficient value of 2000 [W/m2K].

Highlights

- Introduction of a novel AB_2-type Nanomaterial for Hydrogen Storage
- Validated Numerical Model with Solid Experimental Results
- Effective Heat Management
- Stationary Applications for Green Buildings